An-Najah National University
Faculty of Graduate Studies

CdS Thin Film Photo-Electrochemical Electrodes: Combined Electrochemical and Chemical Bath Depositions

By
Sahar Mustafa Asad Khudruj

Supervisors
Prof. Hikmat Hilal
Co-Supervisor
Dr. Iyad Saadeddin

This Thesis is Submitted in Partial Fulfillment of the Requirements for the Degree of Master of Science in Chemistry, Faculty of Graduate Studies, An-Najah National University, Nablus, Palestine.
2011

CdS Thin Film Photo-Electrochemical Electrodes: Combined Electrochemical and Chemical Bath Depositions

By
Sahar Mustafa Asad Khudruj

This thesis was defended successfully on 13/10/2011, and approved by:
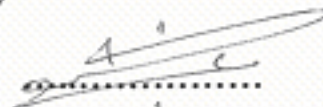
Defense Committee Members   **Signature**

1. Prof. Hikmat Hilal / Supervisor

2. Dr. Iyad Saadeddin / Co-Supervisor

3. Dr. Atef Qasrawi / External Examiner

4. Dr. Ahed Zyoud / Internal Examiner

Dedication

To my mother ……………..

To my uncle Kaid Ata……..

To those who are looking forward for more knowledge……

Acknowledgments

The author wishes to express her sincere appreciation to her supervisors Professor Hikmat S. Hilal and Dr. Iyad Saadeddin for their guidance, help and their moral support throughout research work and writing up.

The author would like to thank Dr. Ahed Zyoud for his help and encouragement throughout research work. Technical help from Chemistry Department Laboratory staff at An-Najah N. University is acknowledged.

Thanks are extended to Dr. DaeHoon Park, (Dansuk, Korea) for help with SEM and XRD measurements. Thanks are also due to Dr. Guy Campet (ICMCB, Bordeaux University, France) and his group for allowing us to use laboratory and equipment. Financial support for this project from Al-Maqdisi program is acknowledged.

I wish to express my appreciation to the patience and encouragements given to me by my family.

Sahar

الإقرار

إنا الموقعة أدناه مقدم الرسالة التي تحمل عنوان

CdS Thin Film Photo-Electrochemical Electrodes: Combined Electrochemical and Chemical Bath Depositions

أفلام CdS الرقيقة كأقطاب فوتوكهروكيميائية: التحضير بالجمع بين الترسيب الكيميائي والكهروكيميائي

اقر بان ما اشتملت عليه هذه الرسالة إنما هو نتاج جهدي الخاص ، باستثناء مـــا تمـــت الإشارة إليه حيثما ورد، وان هذه الرسالة ككل من أو جزء منها لم يقدم من قبل لنيل أية درجـــة أو بحث علمي أو بحثي لدى أية مؤسسة تعليمية أو بحثية أخرى .

Declaration

The work provided in this thesis, unless otherwise referenced, is the researcher's own work, and has not been submitted elsewhere for any other degree or qualification.

Student's name: **اسم الطالبة:**

Signature: **التوقيع:**

Date: **التاريخ:**

List of Contents

List of Tables

List of Figure

**CdS Thin Film Photo-Electrochemical Electrodes: Combined
Electrochemical and Chemical Bath Depositions
By
Sahar Mustafa Asad Khudruj
Supervisors
Prof. Hikmat Hilal
Co-Supervisor
Dr. Iyad Saadeddin**

Abstract

Nano-sized CdS films were deposited onto FTO/glass substrates by different techniques, namely: electrochemical (EC), chemical bath (CB) and electrochemical followed by chemical bath (EC/CB) deposition techniques. The latter technique is examined here for the first time. Scanning electron microscopy (SEM), X-Ray diffraction (XRD), photoluminescence spectra (PL) and electronic absorption spectra were studied for different films. Photo-electrochemical (PEC) characteristics of different films, such as photo *(J-V)* plots, dark *(J-V)* plots, conversion efficiency and stability, were all investigated.

Films prepared by different methods showed different SEM images. Electronic absorption spectra for different films were not much different except in PL intensity values.

PEC characteristics for different films showed different behaviors. The EC/CBD films showed higher light-to-electricity conversion efficiency than EC films, but lower efficiency than CBD counterparts. Moreover, the EC/CBD films showed higher values of J_{SC} with time, than either EC or CBD counterparts, which gives an idea about the advantage of the new described films.

The deposited films were modified by annealing at 250°C under N$_2$. Cooling of pre-heated films to room temperature was performed by a gradual slow process. The effect of annealing & slow cooling on film characteristics, such as XRD, SEM, PL, electronic absorption spectra were all measured for different films. Photo-electrochemical characteristics of different films, such as: open-circuit voltage *(V$_{oc}$)*, current density *(J$_{sc}$)*, photo *(J-V)* plots, efficiency and stability, were studied. Films treated by annealing & slow cooling showed higher conversion efficiency than their un-treated counterparts.

SEM images showed that annealing increased the grain size of CdS nano particle in cases of CBD, EC and EC/CBD. XRD measurements showed that annealing lowered the crystallite size for EC-CdS films, whereas annealing enhanced the crystallite size for both CBD-CdS and EC/CBD-CdS films. Photoluminescence spectra were not affected by annealing except in PL intensity values.

In each prepared CdS film, annealing enhanced PEC characteristics, by increasing conversion efficiency and stability. On the other hand, the annealed EC/CBD showed higher conversion efficiency and stability than either the annealed EC or CBD films.

On the other hand, the higher conversion efficiency of both annealed CBD-CdS and EC/CBD-CdS films than non-annealed counterparts coincided with SEM topography, XRD spectra and PL intensity results. XRD patterns showed enhancement in crystallite size for both annealed

CBD-CdS and EC/CBD-CdS films. SEM images showed homogenized layers with more ordered and uniformly packed coagulates for annealed films. In addition, PL spectra for annealed films exhibited higher emission values than non-annealed films. This is because annealing enhances the particle characteristics, giving more uniform and compact surface and consequently higher PL intensity.

The results indicate that the new CdS nano-films, prepared by EC/CBD technique, are advantageous over other earlier known types.

Chapter One

Introduction

Chapter One
Introduction

1. 1 Potential of Solar Energy

In recent years, the world faced scenario of global warming, ozone layer depletion, impending shortage of fossil fuel sources and serious environmental pollution made by the combustion of fossil fuel. Therefore, the world force to make a lifestyle change to protect the environment and take care of human needs, therefore human look towards one of the most abundant and efficient energy and it is the sun light [1-3].

The Sun radiates about 1.6 x 10^7 watts of power per square meter from its surface at all wavelengths, but this value is reduced vastly as it reaches earth surface. The earth receives 174 peta watts (PW) of incoming solar radiation at the upper atmosphere. Most of the absorption of the sun light occurs after it enters the earth atmosphere. About 30% is reflected back to space while the rest is absorbed by chemical species such as ozone, water vapor and carbon dioxide. The spectrum of solar light at the earth surface is mostly in the visible and near infrared ranges with a small part (~5%) in the near ultraviolet light [4]. Figure (1.1) shows a plot of the percentage of the sun energy that gets transmitted through the atmosphere versus wavelength on a cloudless day.
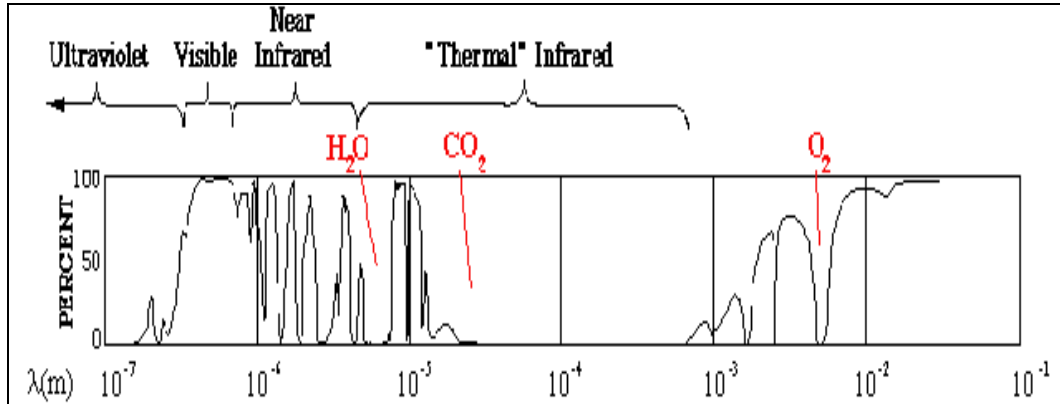
Figure (1.1) Sunlight transmitted through the atmosphere versus wavelength (*Source: NOAA*) [4].

Only about 50% of the sun energy that makes it to the top of the atmosphere actually gets down to the surface, so, sunlight reaches the earth in a quality that is sufficient to supply the total global energy consumption[5].

1.2 Why is Solar Energy Important?

Solar energy has gained a growing interest because of its advantages that make it the main source in light-to-electricity conversion. Its advantages include:

a) solar energy is unlimited natural source.

b) freely available and cleanest energy source.

c) solar energy does not require expensive distribution networks [6].

d) it is the quietest form of energy available and it does not threaten plants and animals.

On the other hand, there is a slow deployment in solar technologies, due to: **firstly**, the intermittent nature of the energy input, which requires energy storage systems to match the energy supply with the electricity demand. **Secondly**, the current high production cost of conventional solar cells compared with other fossil fuels (the cost of active material and the manufacturing techniques). This is the main reason why fossil fuels are used today, in spite of the negative impact they make on the environment [7]. Therefore, it is necessary to explore a new processes for producing low-cost techniques, less expensive materials and suitable for solar cells for electricity production purposes.

1.3 Solar Energy Conversion Technologies

Solar energy can be utilized by using many active technologies to convert it into various energy carriers for further utilization. Figure (1.2) summarizes solar energy conversion processes.
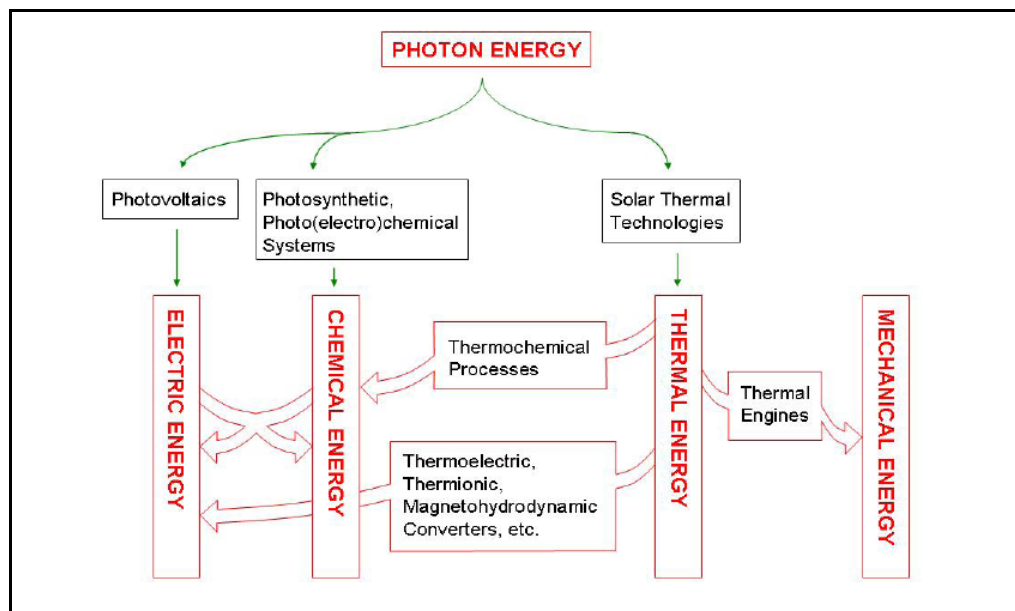
Figure (1.2): Solar energy conversion paths and technologies [8].

1.4 Types of Solar Systems

Technology allows solar energy to be converted into electricity through photovoltaic devices and solar thermal heat. These methods utilize the sun without producing by-products or pollution hazards.

1.4.1 Solar Thermal System

This system uses sunlight in order to boil water in turbine generators. In order to boil water using sunlight, the light must be concentrate from a large area into a very small area. Therefore, light intensity is magnified by using curved mirrors to reflect the light to a focal point.

Solar thermal systems have efficiencies comparable to those of coal or natural gas powered plants. However, thermal systems have main impediment to widespread use and demand high cost of construction and upkeep. Its cost is 1.2-2 times that of coal or nature gas. The price on these systems has been coming down, but it must continue to come down in order to make them economically feasible. There are different design types of solar thermal systems. In **active solar heating system** in which collectors called solar panels are used, while **passive solar heating system** occurs naturally without the use of additional equipment. Both methods involve solar heat to be used to heat water, Figure (1.3). Active solar technologies increase the supply of energy and are considered supply-side technologies, while passive solar technologies reduce the need for alternate resources and are considered demand-side technologies [4].
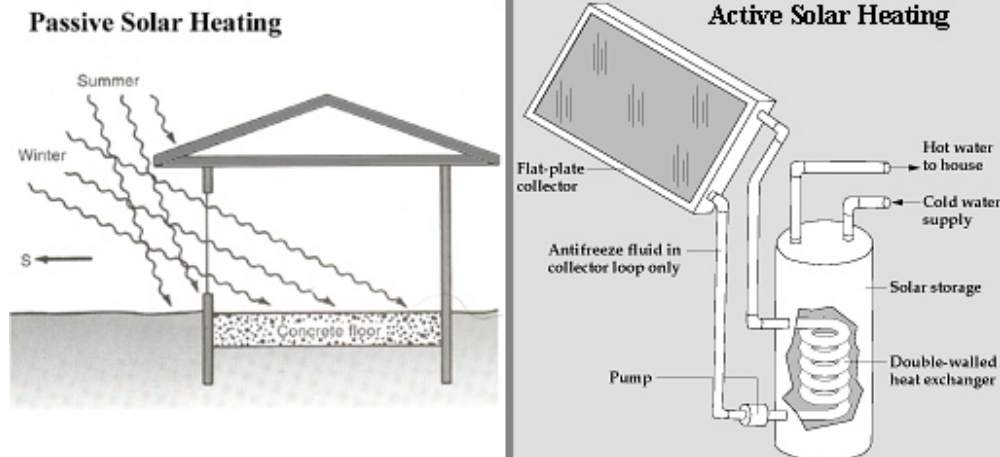
Figure (1.3): Example diagrams for active and passive solar heating systems (*Source: DOE*),[4].

1.4.2 Photovoltaic Devices (PV)

Photovoltaic cells are one type of solar systems that uses the solar energy and converts it directly into electricity via photoelectric effect. Photovoltaic panels have a drawback and low efficiency in the 10-20% range. The low efficiencies are due to [4]:

a) not all frequencies of light are able to free electrons from atoms in the cell.

b) those frequencies of light that are able to free electrons from the atoms do not do in a 100% efficient manner.

Therefore, PV cells create electricity at about 3-5 times the cost of coal or natural gas powered electrical plants. PV cells are based on using semiconductor materials in solar energy conversion into electricity in which a solid–solid junction (p-n junction) is used as the active layer, Figure (1.4). This device involves a semiconductor (SC) which is p-type in

one part and n-type in the other. Separated positive and negative charges $(e^{-}h^{+})$ are create in an electrode in case of absorbed light. Electrons move downhill to n-type through the solid junction and holes move upward towards p-type side by using electrostatic force [9].
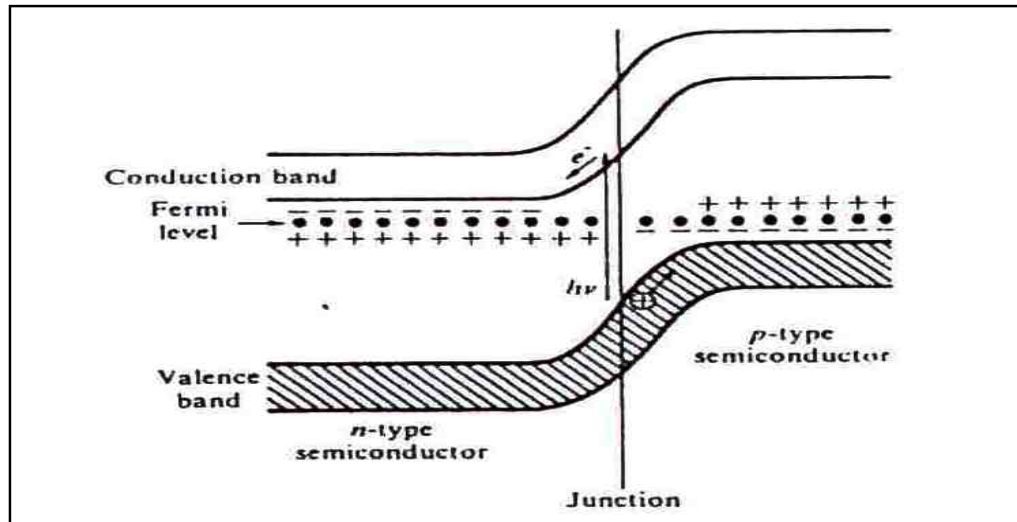
Figure (1.4): Energy level diagram for a *p-n* junction, showing band bending and the creation of an electron-hole pair upon absorption of a photon with wavelength equal or shorter than threshold wavelength (reproduced from ref. [10]).

1.4.3 Photo-Electrochemical Cells

Photo-electrochemical (PEC) cells are based on using semiconductor materials in solar energy conversion into electricity, in PEC cells a semiconductor-electrolyte junction is used as active layer, Figure (1.5).
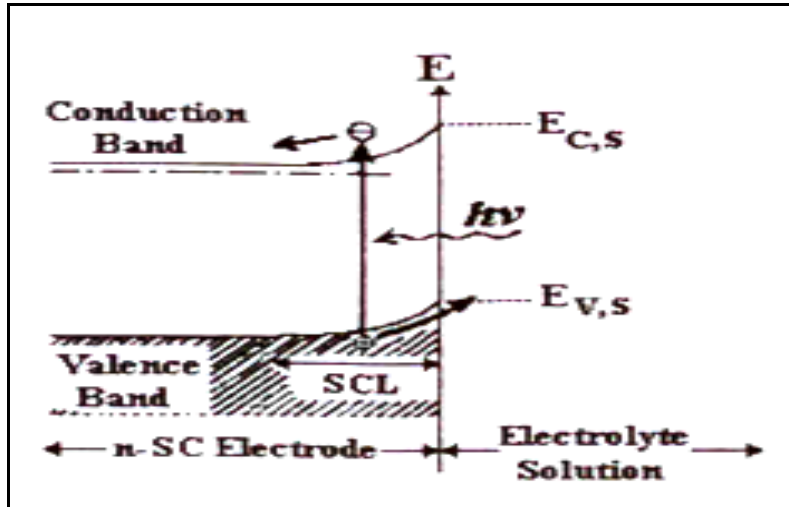
Figure (1.5): Energy level diagram for SC/electrolyte interface showing band bending and the creation of an electron-hole pair in *n*-type SC upon absorption of a photon with wavelength equal or shorter than threshold wavelength. $E_{c,s}$ and $E_{v,s}$ mark the surface energies of the conduction and valence edges respectively (reproduced from ref. [11]).

The semiconductor that is used in PEC cell must be photosensitive, to absorb photons with wavelengths equal or shorter than their threshold wavelength. This is necessary to excite the electrons from the upper valence band to the lowest conduction band. This process creates excess electrons in the conduction band and excess holes in the valence band [12].

PEC techniques in light conversion are generally more economic than PV techniques, and have several advantages compared with PV devices [13], such as:

a) PEC cells can be fabricated and modified with considerable ease.

b) PEC devices can store energy in the form of conventional fuel and can convert light to electrical energy as well.

c) Solution based techniques provide large areas and low cost compared with PV, the areas of which are limited by the sample size and high manufacturing cost.

Relatively high efficiencies have already been achieved in PEC solar cells compared to conventional PV cells. However, there are some material problems that need to be solved before the large-scale commercial exploitation of PEC cells. Examples are photo-corrosion and development of large area polycrystalline semiconductor electrodes [14].

1.4.3.1 Principles of PEC Cells

In the past few years, special attention has been paid to study PEC behavior of polycrystalline semiconductors for possible application in electrochemical solar cells. Junctions in PEC cells are simple to build by simple immersion. Better junction quality, between crystalline solids and liquids, can be made based on better understanding of general basics of PEC cells.

As mentioned previously, PEC cells are based on the formation of an SC-electrolyte junction. When an SC is immersed in a suitable electrolyte solution, a depletion layer (space charge layer, SCL) is formed as a result of n-type SC-electrolyte junction.

In SC, the Fermi level (E_f) is determined by chemical potential of electrons (majority carriers). In solution, the initial chemical potential is determined by the nature and concentration of redox couple electrolytes, Figure (1.6) [15].
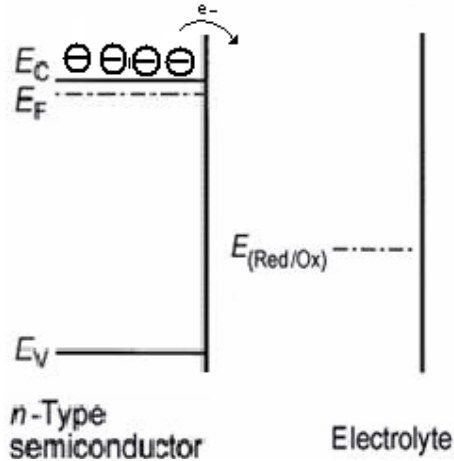
Figure (1.6): *n*-type semiconductor with E_C = lower conduction band edge; E_V = upper valence band edge; E_F = Fermi level; $E_{Red/Ox}$ = standard redox potentials.

When an n-type SC is immersed in a suitable electrolyte, the following energetics will occur. Before equilibrium, the E_f will remain above E_{redox}. Electrons will therefore flow down to E_{redox}, as shown in Figure (1.7a). As a result, E_f will be lowered. The electrons flow will continue until the equilibrium is established, Figure (1.7 b).

At equilibrium, E_f and E_{redox} will match up. This produces a positive SCL in the SC because of chemical reduction process $A^{+2} + \bar{e} \rightarrow A^{+}$ which will produce an electric field in the depletion layer. As a result, conduction and valence band edges are bent and a potential barrier is established against further electron transfer into the electrolyte [16].
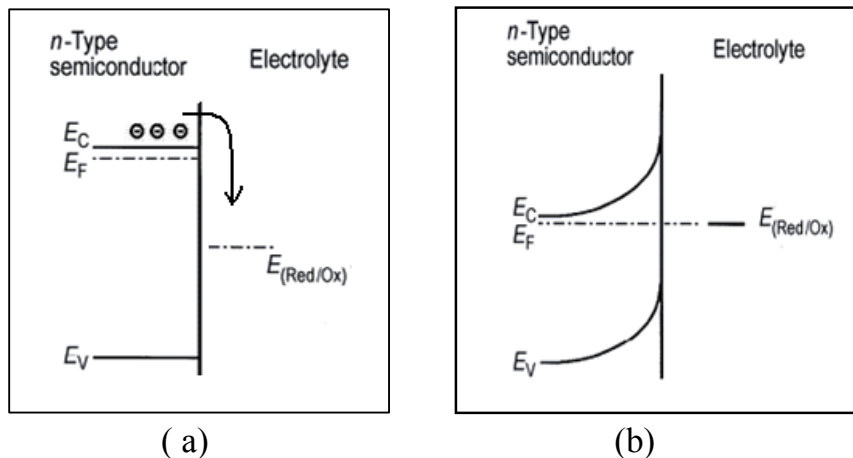
Figure (1.7): *n*-type SC/electrolyte junction in the dark (a) before equilibrium (b) at equilibrium. E_C = lower conduction band edge; E_V = upper valence band edge; E_F = Fermi level; $E_{Red/Ox}$ = standard redox potentials.

In PEC cells, when the SC is exposed to light with energy greater than band gap, this light is absorbed within the SCL of the electrode. The resulting ($\bar{e}$-h^+) pair is split apart. The minority carriers (h^+) will go to the interface. The majority carriers ($\bar{e}$) will move into the bulk of the SC electrode, Figure (1.8) [17].
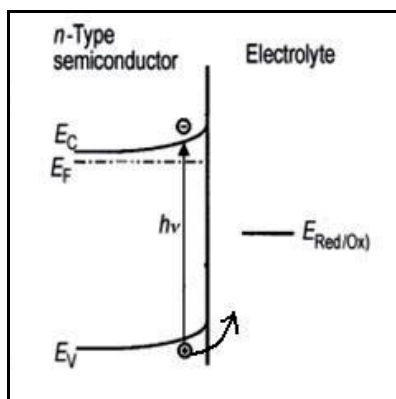
Figure (1.8): Photo voltage formation under illumination. E = electron potential; E_C = lower conduction band edge; E_V = upper valence band edge; E_F = Fermi level; $E_{Red/Ox}$ = standard redox potentials.

Consider an n-type SC and a counter electrode, both in contact with the same electrolyte containing a redox couple. This type of PEC cells is called regenerative cell, Figure (1.9).
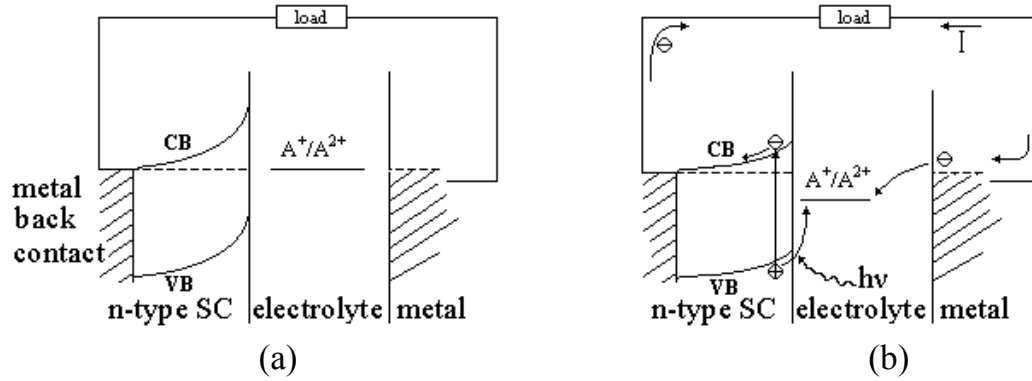
Figure (1.9): energy level diagram regenerative cell at a) equilibrium, and b) during illumination.

At equilibrium, the E_f of the SC and the redox potential of the electrolyte are adjusted in the same level [18-19]. Under illumination, the E_f of both SC and the counter electrode will rise. The excited electrons will move through the external circuit to the counter electrode and reduce the electrolyte,

$$e^- + ox^+ \rightarrow red$$
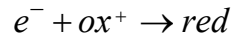
while the holes in the valence band will move to the SC surface and oxidize the reduced species to ox^+ form of the same redox couple in the electrolyte,

$$h^+ + red \rightarrow oxd.$$

The photo-current in the external circuit, resulting with no applied potential is so-called short-circuit current (I_{SC}). The value of I_{SC} can easily be measured [20].

1.4.3.2 Dark Current in PEC Cells

In the dark, at equilibrium, there is a potential barrier that is established against electron transfer between the surface and the bulk of the electrode. This appears as bending the conduction and the valence edges. Band bending in both valence band (VB) and conduction band (CB) represents this potential. Occurrence of dark current is achieved only by applying a negative potential (ΔE_1) to provide electrons with enough energy to overcome this barrier. The electrons are then able to transfer from the n-type SC conduction band to the electrolyte through the interface. Consequently, the SCL disappears and a state of flat band potential occurs, Figure (1.10), [20].
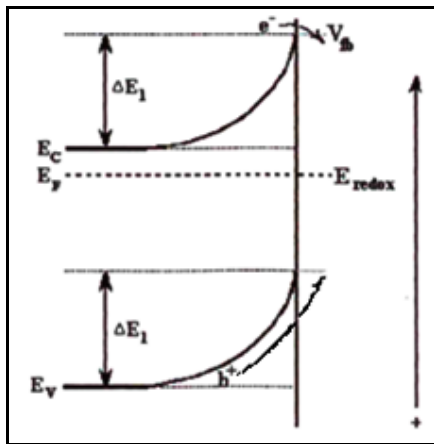
Figure (1.10): Dark current for *n*-type SC.

1.4.3.3 Photocurrent in PEC Cells

When light absorption generates a population of excited holes and electrons, the majority carrier concentration changes relatively little and the minority carrier concentration is greatly enhanced. Hence photo-effects are greatest when minority carriers dominate the electrode response. This occurs when the electrode is biased to form a depletion layer (with positive potential) and the photo-generated minority carriers migrate towards the electrode/electrolyte interface [21].

The SC exhibits a threshold response to photon energy dictated by the band gap energy. The photo-effects switch on as the wavelength of incident light (λ) becomes shorter than the threshold wavelength (λ_g); with λ longer than λ_g the electrode is relatively insensitive to light. A useful relation between the threshold wavelength λ_g and the band gap energy E_g [22] is:

$$\lambda_g = 1240/E_g \tag{1}$$

where λ_g has units of nanometers, and E_g units of electron-volts (eV).

The dependence of the photocurrent or photopotential on excitation wavelength provides information about the band gap energy E_g and nature of optical transition (direct or indirect). *Recombination* is another important phenomenon of photo-effects in the PEC. Recombination can occur directly with the electron descending from the conduction band edge to the hole at the valence band edge, or indirectly via intermediate energy levels

(bulk or surface states). Recombination reduces the magnitude of photo-effect, and consequently lowers the power and the efficiency of PEC cell. When *n*-type SC electrode is biased sufficiently positive of V_{fb} (flat band potential) the dark currents are very low, due to the blocking effect of the depletion layer. Upon irradiation of SC through the electrolyte with light (λ shorter than λ_g), large anodic photocurrents appear, Figure (1.11), [20].
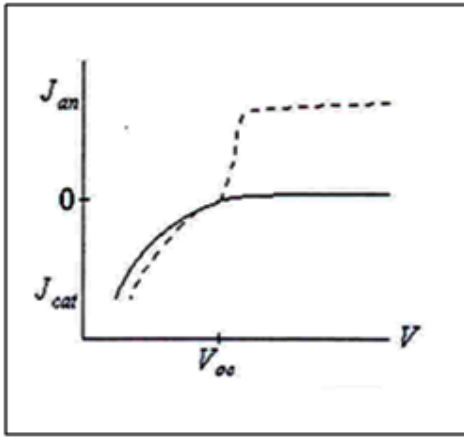
Figure (1.11): Dark and photo current voltammogram for *n*-type SC. J_{an} = anodic current density; J_{cat} = cathodic current density; V_{oc} = open circuit potential; (—) dark current; (---) photo current.

These photocurrents arise from the flux holes (minority carrier) arriving at the surface. The generated electron-hole pairs in the depletion layer are separated by the electric field in the depletion layer, with the electron moving towards the bulk of the crystal and the hole migrating towards the surface, Figure (1.12). Electron-hole pairs generated beyond the depletion layer also diffuse into the electric field and become separated. The shape of the photocurrent voltammogram depends on the energy distribution of the incident photons, the absorption coefficient of the SC, the diffusion distance of the excited holes and electrons and the recombination rates [20].
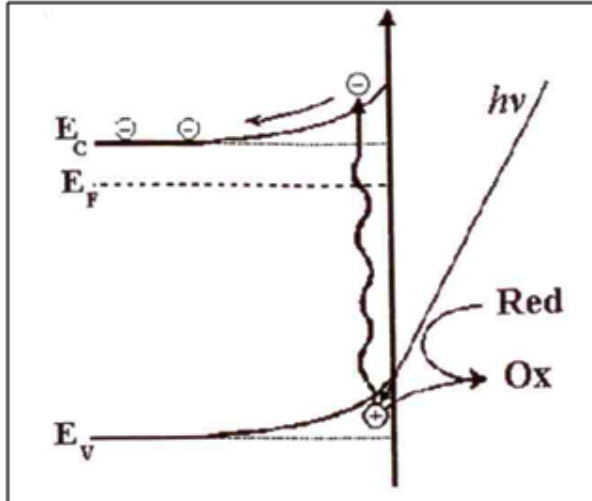
Figure (1.12): Photocurrent generation at *n*-type SC. V more positive than V_{fb}; a depletion layer is formed. Photogenerated holes move to the surface and oxidize solution resultants.

As the applied potential approaches V_{fb} the space charge layer thickness decreases. Recombination rates increase because the holes and electrons are no longer being separated by the electric field. The photocurrents drop sharply and merge with the dark current near V_{fb}, the electrode is no longer blocking, and the dark current increases dramatically, with small cathodic photocurrent sometimes observed [20].

1.5 Semiconductors

Semiconductor (SC) is a material that conducts the electrical current due to electron flow and it is intermediate in magnitude between conductor (that conducts the electrical current easily) and insulator (does not conduct electrical current under normal conditions). Semiconductors are used in modern electronics, including computers, radio, telephones, solar cells and many other devices. Semiconductor solar PV panels or PEC cells directly convert sunlight into electrical current.

In semiconductors, current is often planned as being carried either by the flow of electrons or by the flow of holes "positively charged" in the electron structure of the material, but actually in both cases only the electrons move [23].

In this work we choose poly-crystalline SC in preparation process rather than mono-crystalline SC. That is because thin film SC is easy to prepare with low cost, and demands less amounts of materials compared to mono-crystalline systems. Poly-crystalline SC materials thus help save cost, energy, materials and environment.

1.5.1 General Properties of Semiconductors

Semiconductors are characterized by their flat band potential and energy band gap (E_{bg}) values (the distance between valence band and conduction band). Semiconductors absorb photons having energies greater than their band gap energies. This causes electron movement from the valence band to conduction band leaving behind a positively charged hole.

Semiconductor band gaps are inherent material properties and are difficult to alter. However, the band gap of a semiconductor can be controlled via precise size control of the nanocrystal [24].

1.5.2 Popular Semiconductor Materials Used in Solar Cells

The most common semiconductors being used in solar cell technologies can be categorized into [25]:

1- Elements (e .g. Si and Ge).

2-III-V Compounds (e.g. GaAs, GaP and InP) .

3-II-VI compounds (e.g. CdS, CdSe and CdTe).

4- Transition Metal Di- chalcogenides (e.g. $MoSe_2$ and ZrS_2).

5 - Ternary compounds (e.g. $CuInS_2$ and $CdIn_2Se_4$).

6 - Oxide semiconductors (e.g. TiO_2, WO_3 and ZnO).

7 - Zinc phosphides (e.g. ZnP_2).

CdS, one of the II-VI group semiconductors, plays an important role in optoelectronic devices, such as Lasers, light-emitting diodes and solar cells.

1.5.3 CdS in PEC Cells

Cadmium calchogenides (such as CdS, CdSe) are considered one of the most famous SC's that are used in PEC research [25]. Particular interest developed in CdS films because it has suitable band gap ~2.42 eV, high absorption coefficients, important optical properties, ease of fabrication and numerous device applications [26-27]. It is known typically that sulfur is deficient, possessing the sulfur vacancies with a high electron affinity, this causes CdS to acquire electrons easily, resulting in the material of n-type in nature [26].

CdS exists in two crystalline forms: hexagonal (wurtzite) phase, Figure (1.13b) and cubic (zinc blende) phase, Figure (1.13a). It is possible to grow CdS films in both these phases depending on the deposition conditions and techniques [28-29].
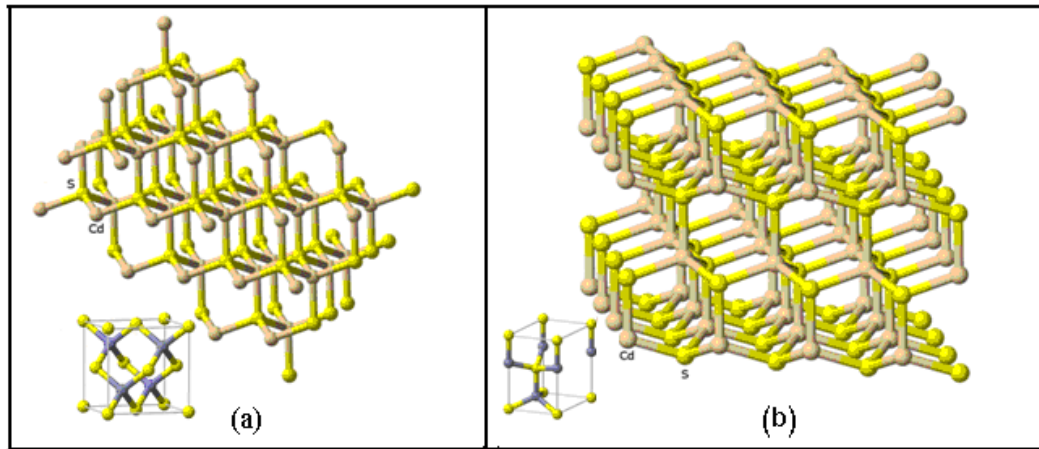
Figure (1.13): a) cubic (zinc blende) structure of CdS. b) hexagonal (wurtzite) structure of CdS [28]

1.6 CdS Thin Film Deposition Techniques

CdS semiconducting electrodes were first used in PEC in the form of a single crystal [30]. Later on, several deposition techniques have been described for obtaining CdS films, in order to fabricate CdS films with desirable electrical and optical properties. Table (1.14) shows a schematic of CdS thin film deposition technologies [31-32].

Table (1.1): Types of CdS thin film deposition techniques [31-32].

CdS deposition techniques	
- Spray pyrolysis.	- Molecular beam epitaxy (MBE).
- Vacuum evaporation.	- Metal organic chemical vapor deposition
- Close space elimination.	(MOCVD).
- Sputtering.	- Close-spaced sublimation (CSS).
- Electrolysis.	- Successive ionic layer adsorption & reaction
- Chemical deposition.	(SILAR).
- Screen printing.	- Pulsed laser ablation.
- RF sputtering.	

CBD and EC techniques were adopted for deposition of CdS thin films, one of common and cheapest methods of preparing CdS thin films, and this is reported in literature [33-36].

1.6.1 Electrochemical Deposition Technique (ECD)

Electro-deposition process is defined as "the process of producing a coating on a cathodic plate electrode by the action of electric current inside an electrolytic cell". This type of deposition (coating) provides some advantages, such as [37]:

(a) surface smoothness.

(b) good performance of protection against corrosion.

(c) low environmental pollution.

(d) ease of processing and thickness control.

(e) ease of condition control such concentrations, pH and temperature.

Therefore, this technique was used here in CdS deposition process onto FTO/Glass substrates. It is assumed also that electrochemical deposition technique makes good contact between CdS film and the FTO/glass substrate surface.

- EC-CdS Growth Mechanism

The electrochemical formation of CdS thin film from a solution containing sulfur on different substrates (TO, ITO, Mo) was described by different researchers [38-39]. It has been found that the resulting electrodeposited CdS thin films appeared uniform and smooth in terms of film quality. The reaction mechanism of CdS formation involves a two electron transfer as follows:

$$Cd^{2+} + S_2O_3^{2-} + 2e^- \longrightarrow CdS + SO_3^{2-}$$
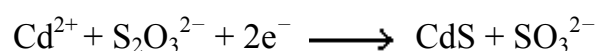
The $S_2O_3^{2-}$ ions react with Cd^{2+} ions, resulting in electro-deposition of CdS layers on the cathode at the proper cathodic applied voltage. Electro-deposition reaction of CdS is dependent of pH, because of disproportion reaction of the thiosulphate ions, which may occur depending on the pH values of the electrolyte, as follows [39]:

$$S_2O_3^{2-} \longrightarrow S + SO_3^{2-}$$
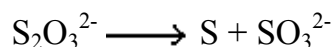
Lowering pH causes the decomposition of $S_2O_3{}^{2-}$ and forms colloidal sulfur, and then sulfer reduced to sulfur ions by accepting two electrons as follows:

$$S + 2\,e^- \longrightarrow S^{2-}$$
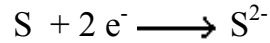
Cd^{2+} ions combined with sulfur ions and precipitated as CdS on cathodic plate as follows:

$$S^{2-} + Cd^{2+} \longrightarrow CdS$$
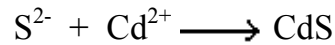
1.6.2 Chemical Bath Deposition (CBD)

CBD technique has proved to be simple, inexpensive, and safe method that procures uniform, adherent and reproducible large area thin films for solar applications [40-41]. On the other hand, CBD technique is not the most efficient polycrystalline thin film deposition technique. However, CBD is competent to be employed for SC electrodes that can be deposited by other techniques, such as electrochemical, to enhance the efficiency.

- CBD-CdS Growth Mechanism

CBD-CdS thin film growth processes have been explained earlier [40, 42-45]. Literature shows that CBD-CdS is based on controlled precipitation of CdS in a bath that CdS deposition takes place by homogeneous (leading to formation of colloids), as well as heterogeneous (on the surface of substrate) reactions [46-47]. The solubility product of

CdS in aqueous media is very small (K_{sp} ~ 10^{-25}) [48]. Therefore, the precipitation control can be achieved by controlling the concentration of free Cd^{2+} ions. And to control the free Cd^{2+} ion concentration, ammonia is used as complexing agent to control the undesired homogeneous reaction. The reaction mechanism of CdS formation is given as [40]:

$$NH_4^+ + OH^- \rightleftharpoons NH_3 + H_2O \tag{1}$$

$$Cd^{2+} + 4NH_3 \rightleftharpoons Cd(NH_3)_4^{2+} \tag{2}$$

$$CS(NH_2)_2 + OH^- \rightleftharpoons SH^- + H_2O + H_2CN_2 \tag{3}$$

$$SH^- + OH^- \rightleftharpoons S^{2-} + H_2O \tag{4}$$

$$Cd(NH_3)_4^{2+} + S^{2-} \rightleftharpoons CdS + 4\,NH_3 \tag{5}$$

$$Cd^{2+} + S^{2-} \rightleftharpoons CdS\,(s) \tag{6}$$
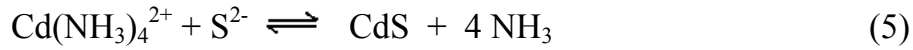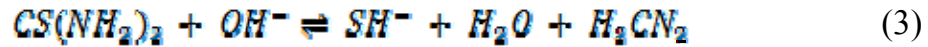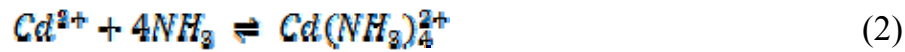
CdS thin films are conventionally deposited onto FTO/Glass by EC or by CBD techniques, but problems in stability and efficiency under PEC conditions are known [49-50]. Therefore, modifications were proposed to enhance efficiency and stability such as annealing & cooling rates.

1.7 Annealing of CdS Semiconductors

Annealing of CdS semiconductor surfaces plays an important role in crystallization process of the semiconductor crystals. It enhances the crystals homogeneity, quality and performance by increasing the efficiency of PEC cells. This is due to the fact that annealing will increase the grain

size, reduce defects in semiconductor and lower surface roughness. Consequently, there is an increase in minority carrier diffusion to electrolyte solution in PEC solar cell [51]. This has been reported in literature [52-60].

1.8 Objectives

The main objective of this work is to prepare a new type of nano-sized CdS film for the purpose of PEC conversion of light-into-electricity. We look for an efficient and stable nano-film under PEC conditions. Therefore, a new preparation technique is proposed here to achieve this goal. The new method involves deposition of CdS nano particles onto FTO/Glass by EC, followed by CBD technique.

Characteristics of nano-sized films, prepared by different techniques, will be compared to find the best methodology giving preferred characteristics. The three preparation techniques are: 1) Chemical Bath deposition (CBD); 2) Electrochemical Deposition (ECD); and 3) The new method using combined EC/CBD technique. Both methods (1) and (2) are known and reported, but the third method is new and has not been investigated before.

The different films prepared by different methods will be compared in terms of: SEM surface topography, XRD crystal structure and PEC characteristics including *J-V* plots, light-to-electricity conversion efficiency, electrode stability, and others. Moreover, effect of annealing & cooling rate on film characteristics will also be studied.

1.9 Hypothesis

CdS which belongs to the II–VI group is one important SC used in photovoltaic and PEC solar cells because of its advantages in having suitable band gap with high absorption coefficients.

Because of inherent defects present in the polycrystalline materials, a considerable portion of the photo-generated charge carriers is lost due to recombination and degradation under PEC conditions. Therefore, considerable efforts are being devoted towards removing these behaviors, hoping to enhance PEC characteristics of the film electrode. It is assumed that our proposed new technique will satisfy this goal. The EC/CBD prepared films are expected to combine advantages of both EC and CBD films.

The EC method is expected to give good contact between the CdS and the FTO surface. The CBD method gives soundly thick layers suitable for light-to-electricity conversion. Therefore, the EC/CBD technique is expected to give a film that has good contact and suitable thickness. However, the EC/CBD method may yield two different distinct layers within the produced CdS film. Such a shortcoming may be avoided by annealing the two layers together and yielding a homogeneous single layer film, with the preferred properties. The final CdS film, prepared by EC/CBD, followed by annealing, is thus expected to give highest conversion efficiency and stability, as compared to earlier EC and CBD

films. To our knowledge, such technique has not been investigated as a tool to enhance the characteristics of CdS thin films.

1.10 Novelty of This Work

In this work, we propose a new technique to prepare CdS films by making combination between EC and CBD techniques. Polycrystalline CdS thin films are prepared by different techniques, namely, EC, CBD, and EC/CBD techniques. All films were deposited onto FTO/Glass. The prepared samples were compared to each other, to obtain the best preparation technique by monitoring different parameters such as: J_{sc}, V_{oc}, efficiency and stability.

The prepared samples will be treated by heating & slow cooling. The effect of such treatment on different parameters for each preparation technique, such as: J_{sc}, V_{oc}, photo J-V plots, stability, SEM and XRD measurements will be investigated in this work.

Chapter Two

Experimental Work

Chapter Two
Experimental Work

2.1 Materials

2.1.1 Chemicals and Solvents

$CdCl_2.2H_2O$, thiourea $(CS(NH_2)_2)$, NH_3, $LiClO_4$, $NaOH$, Na_2S and elemental sulfur were purchased in pure form from Aldrich. HCl, NH_4Cl, $Na_2S_2O_3$ were purchased in pure form from Frutarom. Methanol was obtained from Riedel-DeHaën in a pure form. Highly conductive FTO/Glass samples were kindly donated by Dr. Guy Campet of ICMCB, University of Bordeaux, France.

2.1.2 FTO/Glass Substrate Cleaning Process

FTO/Glass substrates were pre-cleaned before CdS film deposition process, in order to obtain good adherence and uniformity for the deposited CdS films in EC and CBD techniques. The substrates cleaning steps were sequently treated as follows: washing with liquinox soap, distilled water, methanol, washing again with distilled water, then soaking in dilute HCl (10% v/v) for 5 seconds, then rewashing with distilled water, and finally, the substrates were dried in nitrogen atmosphere and inserted in chemical bath.

2.1.3 Preparation of CdS Films

(a) Fabrication of CdS by Electrochemical Deposition (ECD)

CdS films were deposited on pre-cleaned FTO/Glass substrates using EC technique. The major advantages of the electrodeposition technique

are: (i) large area manufacturing. (ii) very low manufacturing cost. (iii) compatibility with a variety of substrates. The experimental arrangement for CdS film preparation is shown in Figure (2.1). It involved a solution containing 10 ml of 0.2 M $CdCl_2$, 10 ml of 0.05 M $Na_2S_2O_3$, small amount of $LiClO_4$, 30 ml of distilled water, HCl to control the value of pH about 2.5 [38-39].

The solution temperature was maintained at 90^oC in a constant temperature oil bath and under constant stirring during deposition [38-39]. The pre-cleaned substrate, with dimensions 1x4 cm^2, and the platinum plate were held by holders and partially immersed in the chemical solution. Teflon sealing was used to isolate metal clamps and wiring.

The system was firmly closed under a continuous flow of nitrogen. Deposition was performed by an applied potential of a DC stripping at different negative potentials (-0.6, -0.7, -0.8, -1.0) V. The best working potential was -0.8 V, and it has thus been used throughout this work unless otherwise stated. Potential control was performed using a 264B model polarography [38].
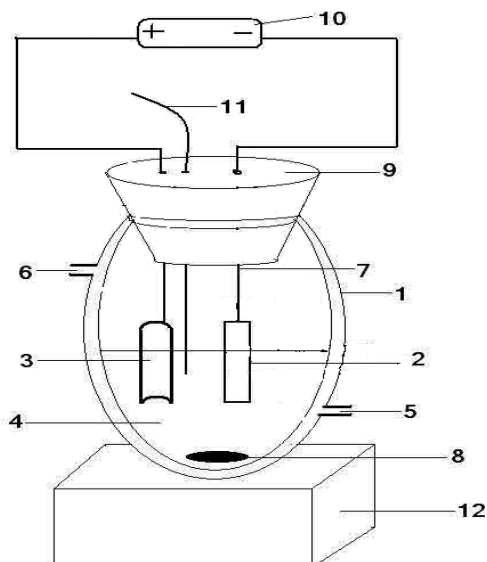
Figure (2.1): Experimental arrangement for CdS film growth

1- Beaker (60 ml) ; 2- FTO/Glass substrate; 3- platinum electrode; 4- solution containing (water, $CdCl_2$, $Na_2S_2O_3$, $LiClO_4$ and HCl); 5- paraffin oil input for the constant–temperature bath; 6-paraffin oil output for the constant -temperature bath; 7-substrate holder; 8-magnetic stirrer; 9-rubber seal; 10- power supply; 11-nitrogen; 12-magnetic stirrer plate.

The substrate was connected to the cathode, and the platinum plate was connected to the anode of the power supply. The best obtained deposition time was 100 minute. During deposition, distilled water (5-6) ml was added after 16 minute from the start, to maintain the volume of the bath solution constant. The coated substrate was cleaned with distilled water and dried with N_2 atmosphere.

b) Fabrication of CdS by Chemical Bath Deposition (CBD)

CdS thin films were deposited on FTO/Glass substrates using CBD technique. The experimental setup for CdS film preparation is shown in

Figure (2.2). It involves a chemical bath containing 25 ml of stirred de-ionized water, $CdCl_2$ (2.50 ml, 0.12 M), NH_4Cl (10 ml, 0.20 M), NH_3 (15.0 ml, 2.00 M). The bath temperature was maintained at 80^oC in a constant temperature water bath under constant stirring during deposition [49].
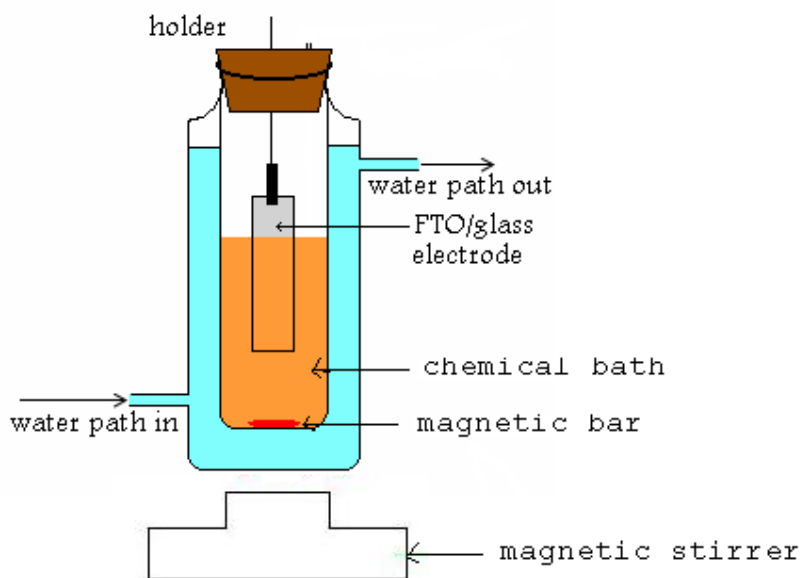
Figure (2.2): Experimental setup for solution growth of CdS film.

The pre-cleaned FTO/Glass substrates, with dimensions 1x 4 cm^2, were held by a substrate holder and covered with Teflon. The substrates were then partially immersed in the solution. The system was firmly closed using a rubber seal.

Finally, thiourea solution (2.50 ml, 0.60 M) was added to the chemical bath. The total volume of the chemical bath mixture became 55 ml, and the final pH was ~10.3. The deposition time was 30 minutes. During deposition, the solution color changed from pale yellow to yellow and finally to bright orange. After deposition, the coated substrate was cleaned with distilled water and dried with N_2 atmosphere.

c) EC/CBD Combined Fabrication of CdS

CdS pre-coated FTO/Glass substrates (by EC) were cleaned with distilled water, soaked in dilute HCl (0.5% v/v, prepared by adding 5 mL of 10% to 95ml distilled water in 100 ml volumetric flask), washed again with distilled water and finally dried with N_2 atmosphere. Then, the CBD technique was applied to the EC prepared CdS film, as mentioned previously. Two layers of non-homogeneous CdS films were thus prepared by the combined technique. Figure (2.3) shows a schematic of the resulting layers of CdS by this method. After deposition, the coated CdS/FTO/Glass substrates were cleaned with distilled water and dried with N_2 atmosphere.
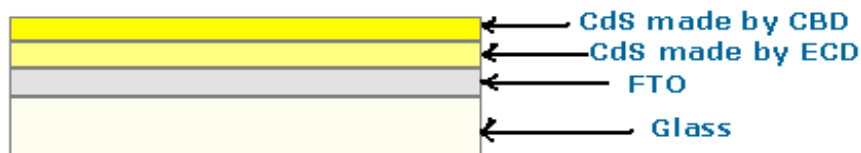
Figure (2.3) A schematic showing CdS/FTO/Glass

substrate prepared by combined EC/CBD technique.

2.1.4 Annealing Process

Film annealing was conducted using a thermostated horizontal tube furnace. The prepared CdS thin film substrates were inserted in the middle of a pyrex cylinder for annealing. Temperature was fixed at 250°C, under N_2 atmosphere for 30 minutes. Figure (2.4) shows a schematic for the tube furnace used.
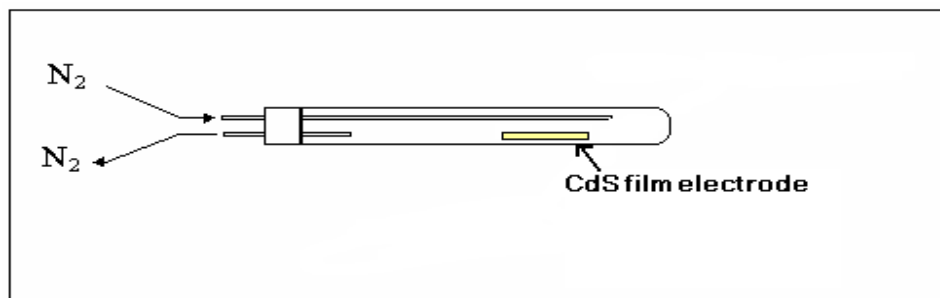
Figure (2.4): The annealing system

2.1.5 Cooling Process

After the film substrates were annealed to the desired temperature for 30 min., the furnace was shut down and left to cool slowly to room temperature under N_2 atmosphere. The time of slow cooling process was about 2 hours with cooling rate 2.08 $^{\circ}$C/min.

2.2 Measurements

2.2.1 Electronic Absorption Spectra

A Shimadzu UV-1601 spectrophotometer was used to measure solid state electronic absorption spectra for different thin films of CdS. A FTO/Glass substrate was used in absorbance measurements as baseline spectra. The wavelength of the incident photons was varied in 300-800 nm.

2.2.2 Fluorescence Spectrometry

A Perkin-Elmer LS 50 luminescence spectrophotometer was used to measure the emission fluorescence spectra for different preparation types of CdS/FTO/Glass substrates. A cut-off filter (500 nm) was used to remove

undesired reflected shorter wavelengths. Emission PL spectra were measured to find the band gap for CdS nano particles.

2.2.3 Scanning Electron Microscopy (SEM)

The SEM was used to study the surface morphologies of our CdS films prepared by different techniques. SEM measurements were kindly conducted in Jung-Eun KIM, ISAA Environment Consulting Co., Ltd., 329-5, Chilgeum-Dong, Chungju-City, Chungbuk, 380-220 South Korea, by using field emission-scanning electron microscopy (FE-SEM, JEOL JSM-6700F) with an energy dispersive X-ray spectrometer (EDS) instrument for measuring purposes.

2.2.4 X-Ray Diffraction (XRD)

X-Ray diffraction technique was used to give information about the crystallographic structure and chemical composition of our CdS thin films prepared by different techniques. XRD measurements of this work were carried out in the ICMCB laboratories, Bordeax University, using a Philips XRD X'PERT PRO diffractometer with Cu Kα ($\lambda_{1.5418Å}$) as a source. The XRD lines were identified by comparing the measured diffraction patterns to JCPDS data-base cards.

2.2.5 Photo-Electrochemical Cell Description

The prepared CdS thin film electrode was incorporated as a working electrode into a two-electrode one-compartment PEC cell, with a platinum counter electrode and reference electrode connected with it, Figure (2.5)
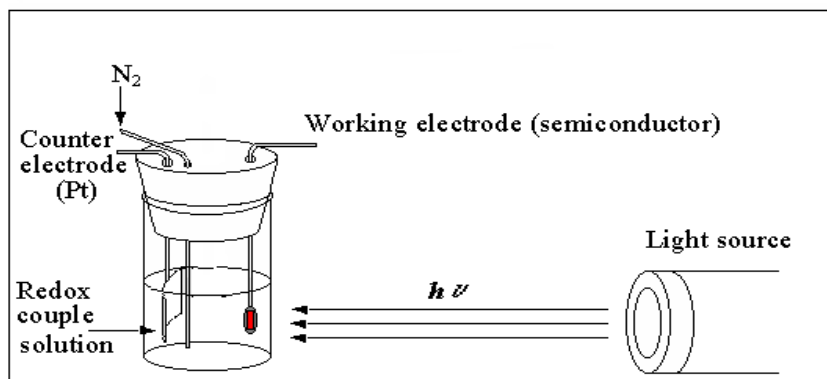
Figure (2.5): Two-electrode photo-electrochemical cell (PEC).

Poly sulfide $NaOH/S^{2-}/S_x^{2-}$ system was used in this experiment as a redox couple (0.1M Na_2S, 0.1 M NaOH, 0.1 M S) [49]. The solution was stirred at the beginning, but stirring was stopped as the PEC experiment started. High purity N_2 gas (99.99999%) was bubbled through the solution for 5 minutes before each experiment, and was kept to flow above the solution during the experiment to minimize air contamination.

A 50 Watt solar simulator halogen spot lamp was used as a light source. The lamp was placed at a defined distance from the working electrode. The halogen spot lamp spectrum was comparable to solar light spectrum as shown in Figure (2.6). The illumination intensity on the electrode was measured by a LX-102 Lightmeter and was ~59000 lux (equivalent to 0.0086 $W.cm^{2-}$).
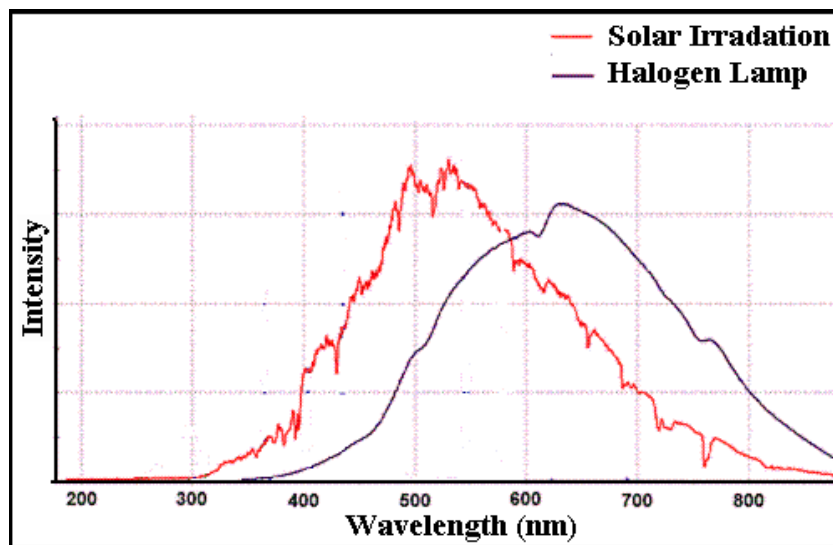
Figure (2.6): Solar radiation and Halogen spot lamp spectrum.

2.2.6 Current Density-Potential Plots

Measurements of current density vs. voltage *(J-V)* plots were performed using a computer controlled Princeton Applied Research (PAR) Model 263A Potentiostat/Galvanostat. Experimental setup mentioned above (Figure 2.5) was used at room temperature under N_2 atmosphere.

The dark current experiments were conducted with complete exclusion of light, by covering the system with a black cloth. On the other hand, the 50 Watt halogen spot lamp was used in measuring photo *J-V* characteristics. Different types of films were compared with each other by monitoring different parameters J_{sc}, V_{oc}, dark *(J-V)* plots and photo *(J-V)* plots, to obtain the best preparation technique.

2.2.7 Electrode Stability Testing

Electrode stability testing experiments were conducted using a Polarographic analyzer (Pol 150) and Polarographic stand (MDE 150). The

PEC cell described above was used to measure value of J_{SC} vs. time, using S^{2-}/S_x^{2-} as redox couple. The temperature was maintained at about $20^{\circ}C$ in a constant temperature water bath, with a continuous flow of N_2.

Values of short circuit current (I_{sc}) were first measured with time, while keeping the electrode under steady illumination ($0.0086\ Wcm^{-2}$) at a 0.00 V vs. SCE. The values of short circuit current density (J_{sc}) were then calculated by dividing the measured short circuit current (I_{sc}) by the measured electrode area exposed. The short circuit current density (J_{sc}) was measured with time, for different types of preparations.

Chapter Three

Results

Chapter Three
Results

3.1 General Remarks

In this study, CdS nano-sized thin films were deposited onto FTO/Glass substrates by different techniques, namely: EC, CBD, EC/CBD techniques. XRD, SEM, PL, electronic absorption spectra and PEC characteristics were all investigated for different films. Moreover, effects of annealing and gradual slow cooling process on film characteristics were studied for different films by monitoring different parameters, such as:

a) XRD measurements.

b) SEM measurements.

c) PL spectra.

d) Electronic absorption spectra.

e) Dark J-V plots.

f) Photo J-V plots.

g) Efficiency enhancement.

h) Value of short-circuit current and stability testing.

The ideal dark J-V plot, Figure (3.1), can be defined as: "a smooth plot in which the current density remains zero for a given potential, and suddenly drops negative at the onset potential (V_{onset})". An ideal photo J-V

plot, Figure (3.2), can be defined as: "a smooth plot in which the fill factor (FF) approaches 1".
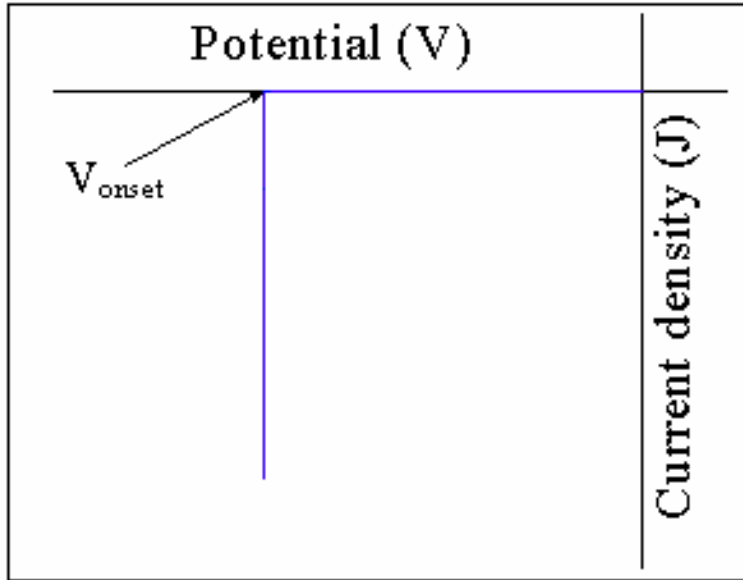
Figure (3.1): Ideal dark *J-V* plot for semiconductors.
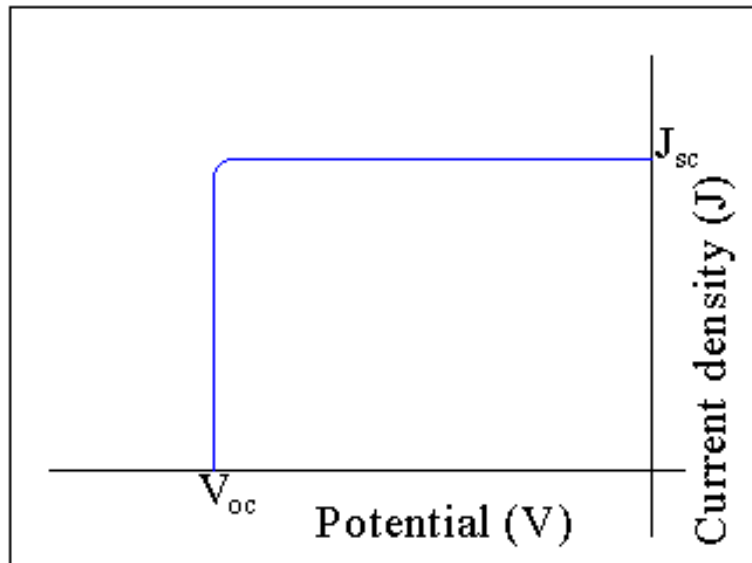
Figure (3.2): Ideal photo *J-V* plot for semiconductors.

3.2 Electrochemically Deposited (EC) Films

3.2.1 XRD Spectra for CdS Thin Film Electrodes

XRD measurements were obtained for EC-CdS films before and after annealing & slow cooling. XRD data showed that both annealed and non-annealed EC-CdS films exhibited crystallinity. X-ray diffraction patterns are shown in Figure (3.3) and Table (3.1). The average grain size of the CdS was estimated by using Debye-Scherrers' formula, $D = 0.9\lambda/\beta\cos\theta$, in which D is the average grain size (Å), λ is the X-ray wavelength, and β is the full-width at half-maxima (FWHM) in radians and θ is the diffraction angle. The average grain size for CdS nano-particles was found to be ~ 61 nm before annealing, as shown in Figure (3.3a), and decreased to ~35 nm after annealing & slow cooling, as shown in Figure (3.3b). The film involved both cubic and hexagonal phases. However, in this study, no measurable phase change in the crystal structure of EC-CdS films after heat treatment in N_2 atmosphere occurred.
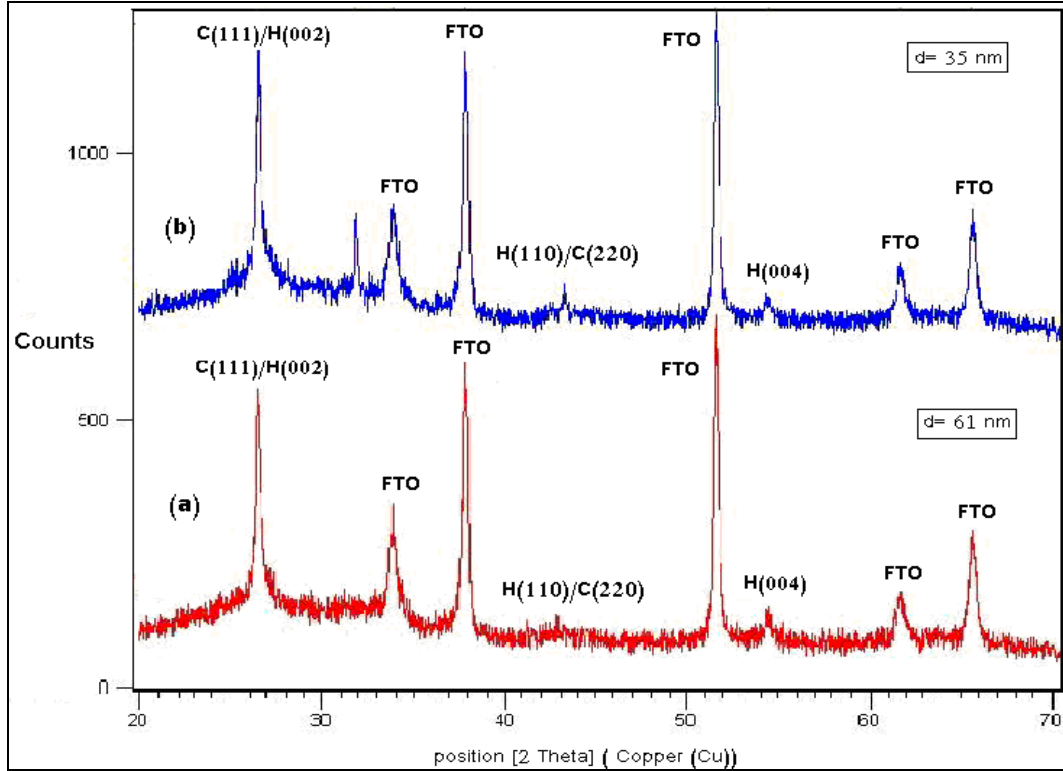
Figure (3.3): X-ray diffraction of EC-CdS films, a) before annealing, and b) after annealing & slow cooling.

Table (3.1): XRD measurements for EC-CdS films before and after annealing.

Position of observed peak (2 theta)	Cubic (C) (h k l)	Hexagonal (H) (h k l)	References
(non-annealed) 26.50	C(111)	H (002)	[61]
33.81	FTO subs.	----	[62]
37.82	FTO subs.	----	[62]
42.77	C(220)	H(110)	[61]
51.54	FTO subs.	----	[62]
54.47	H (004)	----	[61]
61.66	FTO subs.	----	[62]
65.63	FTO subs.	----	[62]
(Annealed) 26.55	C(111)	H (100)	[61]
33.81	FTO subs.	----	[62]
37.88	FTO subs.	----	[62]
43.26	C(220)	H(110)	[61]
51.54	FTO subs.	----	[62]
54.44	H (004)	----	[61]
61.65	FTO subs.	----	[62]
65.84	FTO subs.	----	[62]

3.2.2 SEM Images for CdS Thin Film Electrodes

SEM surface imaging is an important and useful method to study the surface quality of semiconductors. That is because surface quality affects SC performance in PEC processes. SEM surface images were obtained for CdS thin films after annealing/slow cooling, to see the uniformity and quality of the surfaces.

The SEM image for the annealed film showed a surface with coagulates of nano-sized particles. The coagulates exhibited different sizes (0.068- 0.272 μm). The surface topography showed ups and downs, indicating relatively low uniformity.
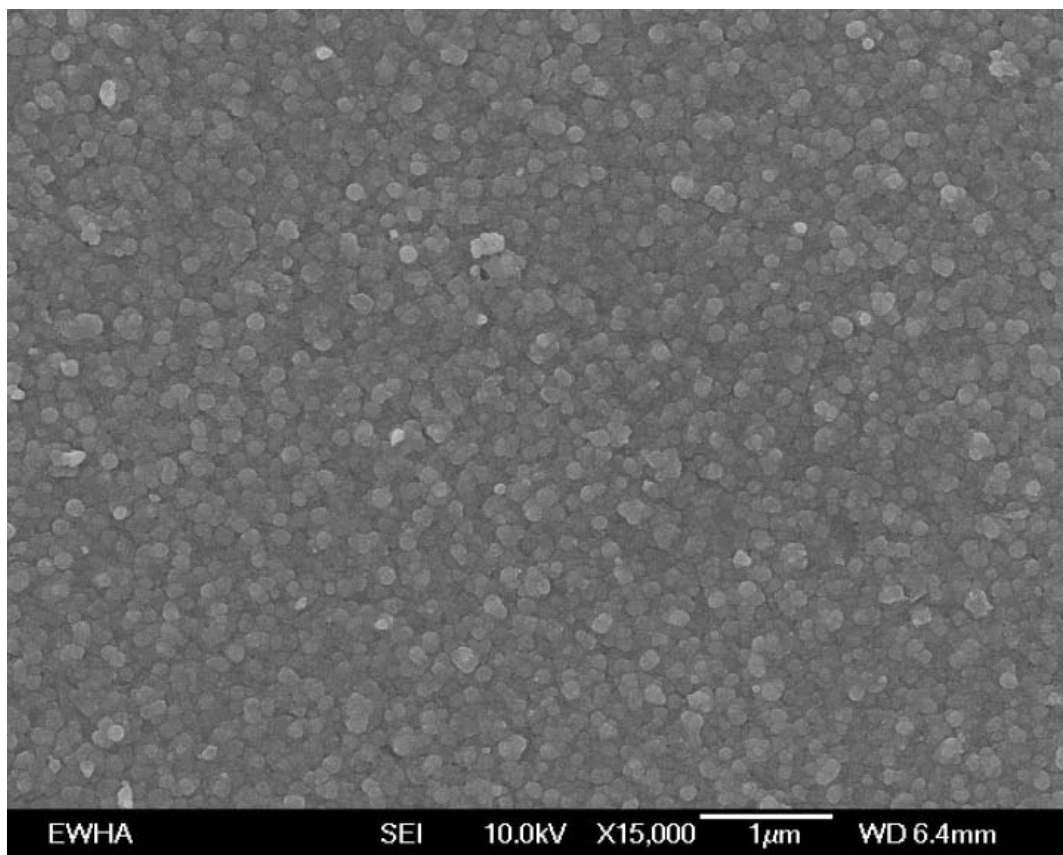
Figure (3.4): SEM surface for EC-CdS thin film after annealing/slow cooling.

3.2.3 Photoluminescence Spectra

Photoluminescence spectra for EC-CdS films were investigated before and after annealing & slow cooling. The system was excited at wavelength ~392 nm. Similar patterns were observed for photoluminescence spectra of EC-CdS films before and after annealing & slow cooling. In both cases, emission intensities appeared at wavelength ~535 nm. The band gap was thus 1240/535 = 2.31 eV. The intensity that appears at wavelength ~600 nm was due to FTO/Glass substrate, as shown in Figure (3.5). The intensity at wavelength ~485 nm was due to surface states that may exist in CdS film. The emission intensity value for annealed electrode was higher than that for non-annealed counterpart. While the PL intensity value for annealed film was ~1.7 (a.u), the non-annealed PL intensity value was ~1.4 (a.u).
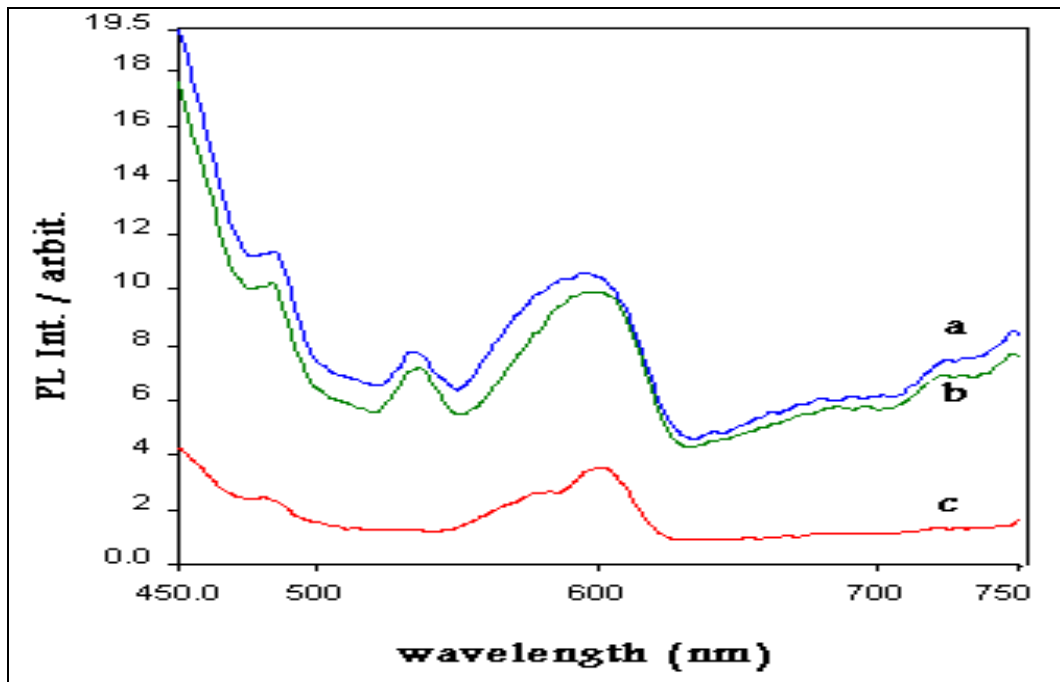
Figure (3.5): Photo-luminescence spectra for CdS/FTO/Glass film a) before annealing, b) after annealing, and c) for FTO/Glass substrate.

3.2.4 Electronic Absorption Spectra

Electronic absorption spectra for EC-CdS were difficult to measure due to the very thin CdS films onto FTO/Glass substrates.

3.2.5 Dark *J-V* Plots of CdS Thin Film Electrodes

In general, non annealed EC-CdS film electrodes showed similar dark *J-V* plots to the annealed EC-CdS film electrodes. Figure (3.6) illustrated the similarity.
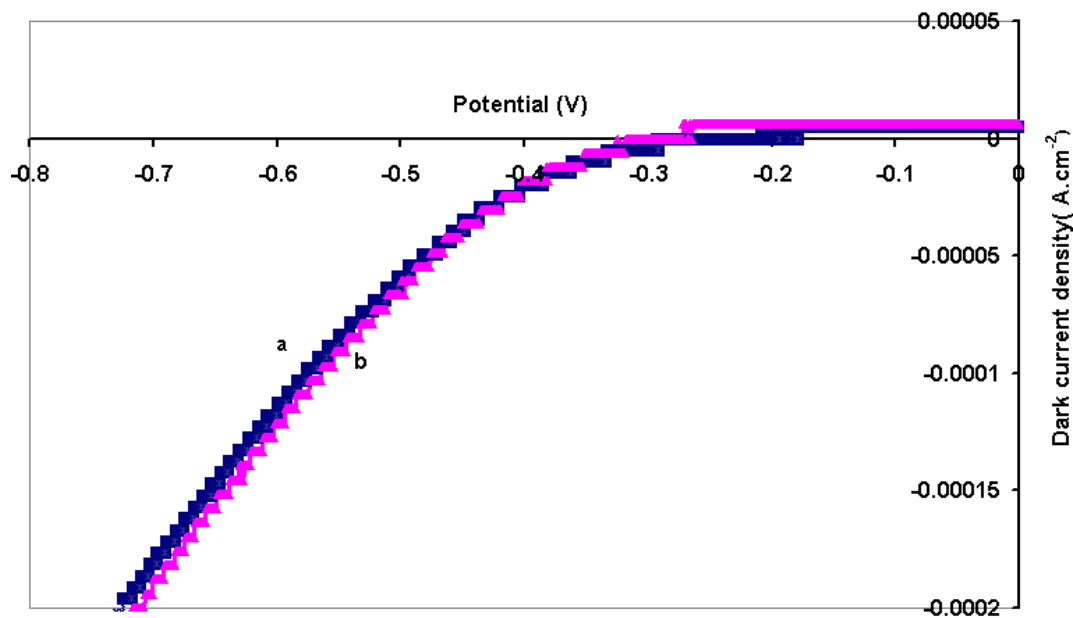
Figure (3.6): Dark *J-V* Plots for EC-CdS film a) before annealing, b) after annealing & slow cooling. All *J-V* measurements were conducted in aqueous S^{2-}/S_x^{2-} redox system at room temperature.

3.2.6 Photo *J-V* Plots of CdS Thin Film Electrodes

Better photo *J-V* plots mean higher J_{sc} value and more negative V_{oc}, which indicates higher theoretical cell conversion power. For nano-sized CdS particles prepared by EC technique, annealed & slow cooled CdS thin

films showed higher J_{sc} than non annealed counterparts. While the annealed films showed J_{sc} ~1×10^{-4} A.cm^{-2}, the non-annealed electrodes showed J_{sc} ~ 5×10^{-5} A.cm^{-2}, Figure (3.7).

Annealed & slow cooled EC-CdS films have percentage conversion efficiency (η %) higher than non-annealed EC-CdS films counterparts. While the annealed films showed (η%) ~0.103%, the non-annealed electrodes showed only ~0.043%. Differences in photo J-V plots for annealed and non-annealed electrodes are consistent with SEM and XRD measurements shown earlier.
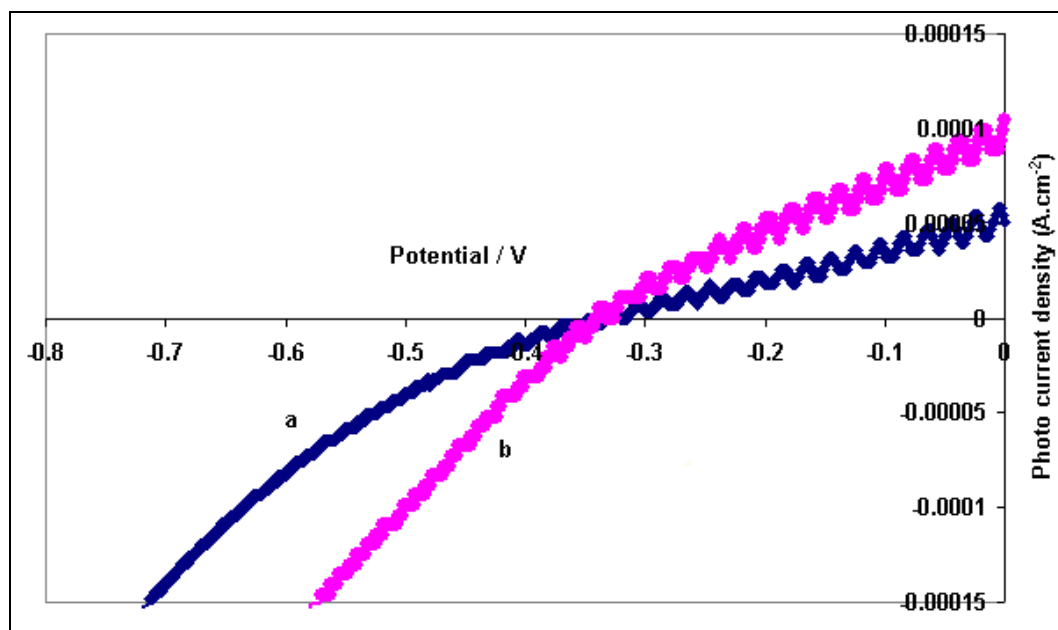
Figure (3.7): Photo *J-V* Plots for EC-CdS film, a) before annealing, b) after annealing & slow cooling. All measurements were conducted in aqueous S^{2-}/S$_x^{2-}$ redox system at room temperature.

3.2.7 Effect of EC-CdS Film Annealing on Electrode Stability

The stability of different EC-CdS thin films, annealed and non-annealed, under PEC conditions has been studied. The value of J_{sc} vs. time

was measured using 0.0V applied potential (vs. SCE). The effect of annealing & slow cooling on J_{sc} vs. time plots has been studied. The annealed & slow cooled CdS films showed higher J_{sc} vs. time than non-annealed CdS film counterpart for as long as 150 minutes. After that, J_{sc} vs. time plots for annealed electrodes went down and coincided with non-annealed electrode J_{sc} vs. time plot. This indicates relative stability of CdS thin films under PEC conditions. Stability study shows no much difference between annealed and non-annealed EC-CdS electrodes, Figure (3.8).
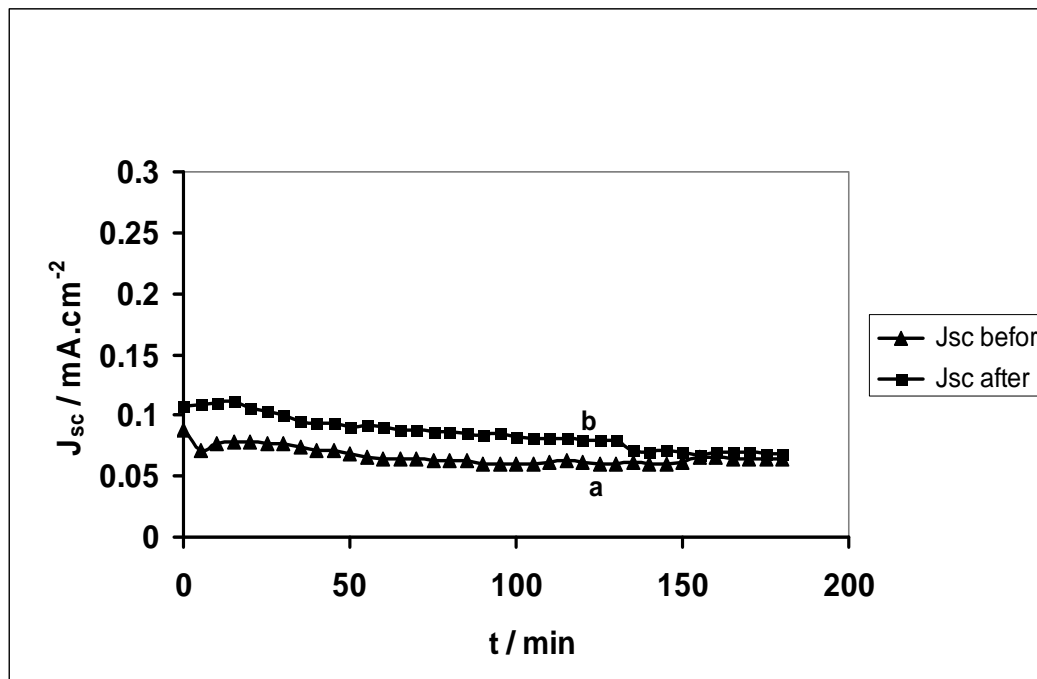
Figure (3.8): short circuit current density vs. time measured for EC-CdS thin film electrodes, a) before annealing, b) after annealing & slow cooling. All measurements were conducted in aqueous S^{2-}/S_x^{2-} redox system at room temperature.

3.3 Chemical Bath Deposited (CBD) Electrodes

3.3.1 XRD Spectra for CdS Thin Film Electrodes

XRD measurements were obtained for CBD-CdS films before and after annealing & slow cooling. XRD data showed that both annealed and non-annealed CBD-CdS films exhibited crystallinity. X-ray diffraction patterns are shown in Figure (3.9) and Table (3.2). The average grain size of the CdS was estimated using Debye-Scherrers' formula. The average grain size for CdS nano-particles was found to be ~ 31 nm before annealing, and increased to ~ 41 nm after annealing & slow cooling, as shown in Figure (3.9a,b). The film involved both cubic and hexagonal phases. However, in this study, no significant change on the crystal structure of EC-CdS films after heat treatment under N_2 atmosphere occurred.
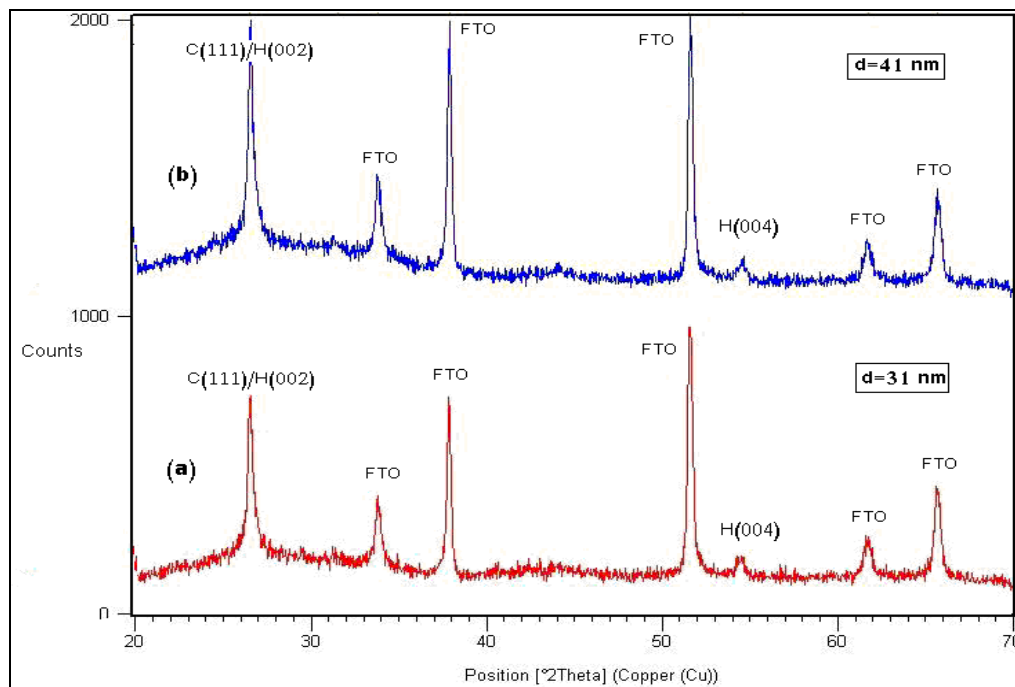
Figure (3.9): X-ray diffraction of CBD-CdS, a) before annealing, and b) after annealing & slow cooling.

Table (3.2): XRD measurements for CBD-CdS films before and after annealing.

Position of observed peak (2 theta)	Cubic(C) (hkl)	Hexagonal (H) (hkl)	References
(Non-annealed) 26.53	C (111)	H (002)	[61]
33.79	FTO subs.	---	[62]
37.86	FTO subs.	---	[62]
51.52	FTO subs.	----	[62]
54.55	H(004)	----	[61]
61.77	FTO subs.	----	[62]
65.64	FTO subs.	----	[62]
(Annealed) 26.53	C (111)	H (002)	[61]
33.79	FTO sub.	---	[62]
37.91	FTO sub.	----	[62]
51.57	FTO sub.	----	[62]
54.53	H(004)	---	[61]
61.68	FTO subs.	---	[62]
65.64	FTO subs.	---	[62]

3.3.2 SEM Images for CdS Thin Film Electrode

CBD-CdS thin films, annealed & slowly cooled to room temperature, showed higher quality surfaces than non-annealed counterparts. Both systems showed SEM images with smaller nano-sized particles, that combine together into larger micro-sized coagulates.

Comparison between SEM images for annealed and non-annealed electrodes, showed that the latter had smaller nano-particles (~35 nm) than the former (48 nm). Moreover, the annealed electrode involved larger and more uniform coagulates than the non-annealed. These observations are shown in Figure (3.10a-b). The coagulates, present in the annealed electrode, Figure (3.10b), are more ordered and uniformly packed than in the non-annealed, Figure (3.10a). This result is consistant with XRD results shown earlier.
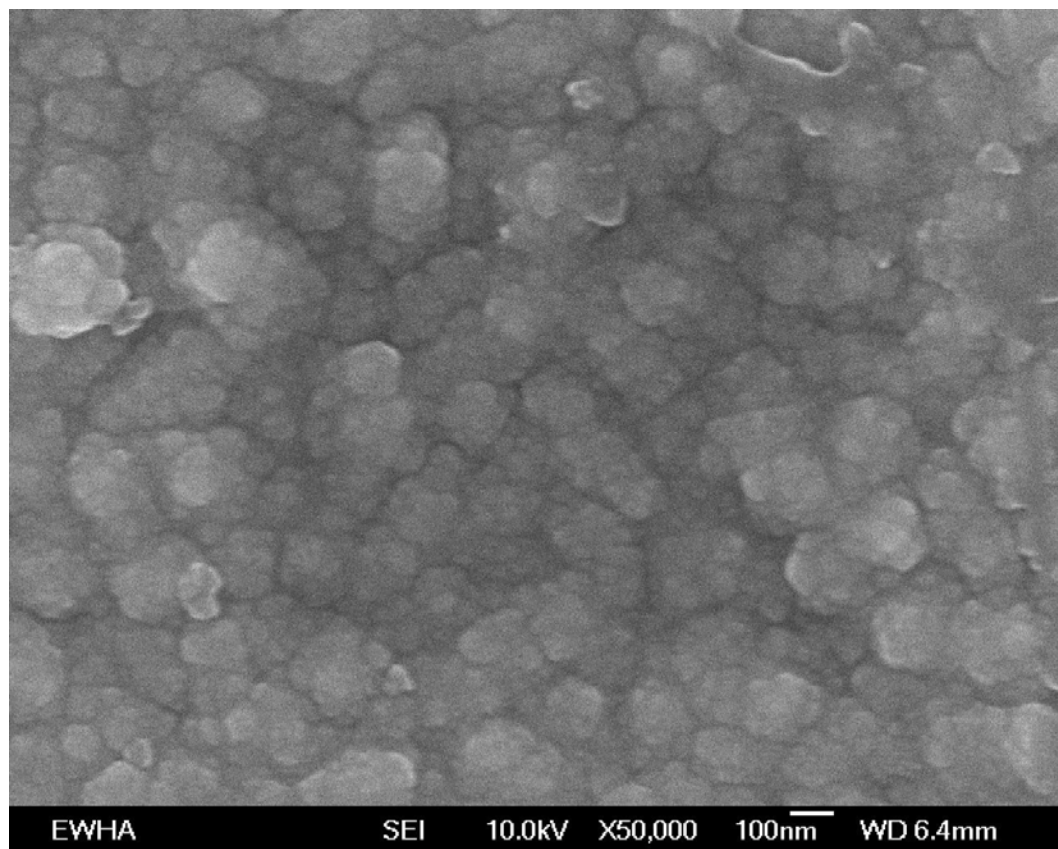
Figure (3.10a): SEM surface for CBD-CdS thin film before annealing.
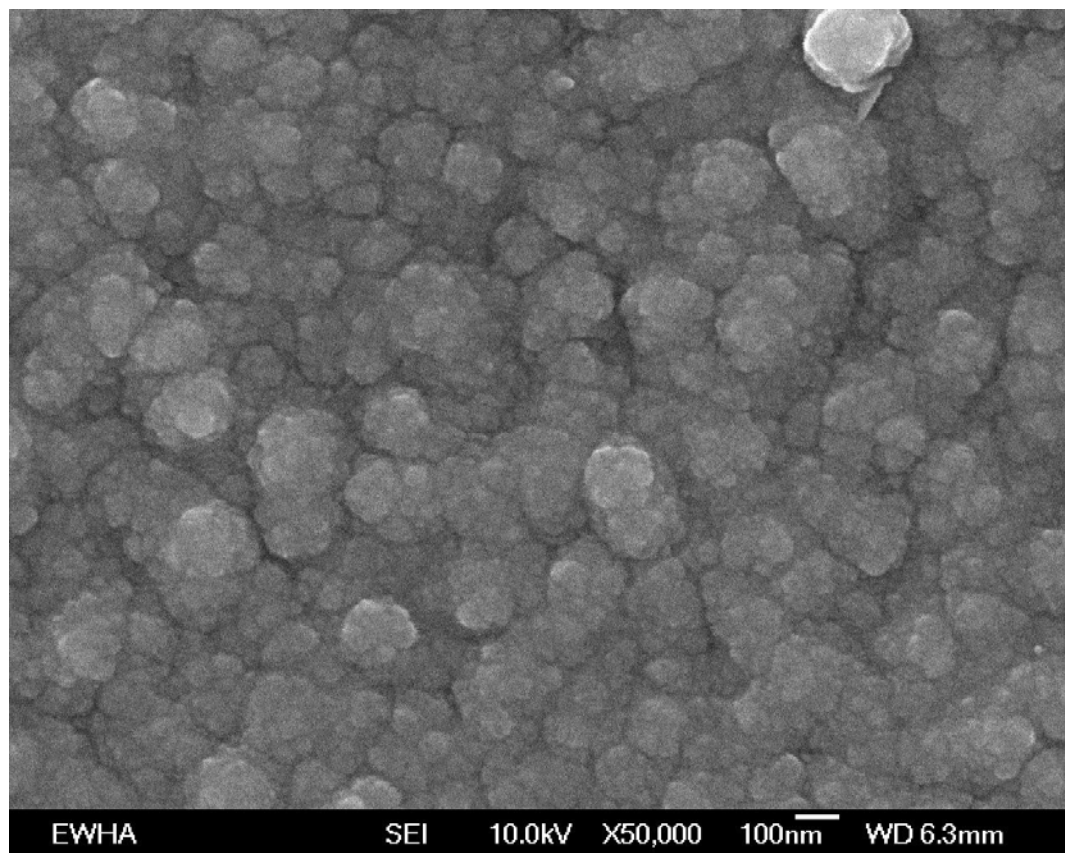
Figure (3.10b): SEM surface for CBD-CdS thin film after annealing & slow cooling.

3.3.3 Photoluminescence Spectra

Photoluminescence spectra for CBD-CdS films were investigated before and after annealing & slow cooling. The system was excited at wavelength ~392 nm. Nearly similar photoluminescence spectral patterns were observed for CBD-CdS films before and after annealing. The highest emission intensities appeared at wavelength ~535 nm, with a band gap 1240/535 = 2.31 eV. The additional band at wavelength ~600 nm was attributed to FTO/Glass substrate. The intensity at wavelength ~481 nm was due to surface states that may exist in CdS film.

Photoluminescence intensity value (~0.625 a.u) for untreated CBD-CdS films was lower than that for the annealed counterpart (~1.1 a.u), Figures (3.11a-b). This indicates that annealing induces enhancement in PL intensity, as a result of enhancement in particle characteristics. The fact that no shifting in maximum emission wavelength occurred indicates no significant change in type of crystalline structure by annealing.
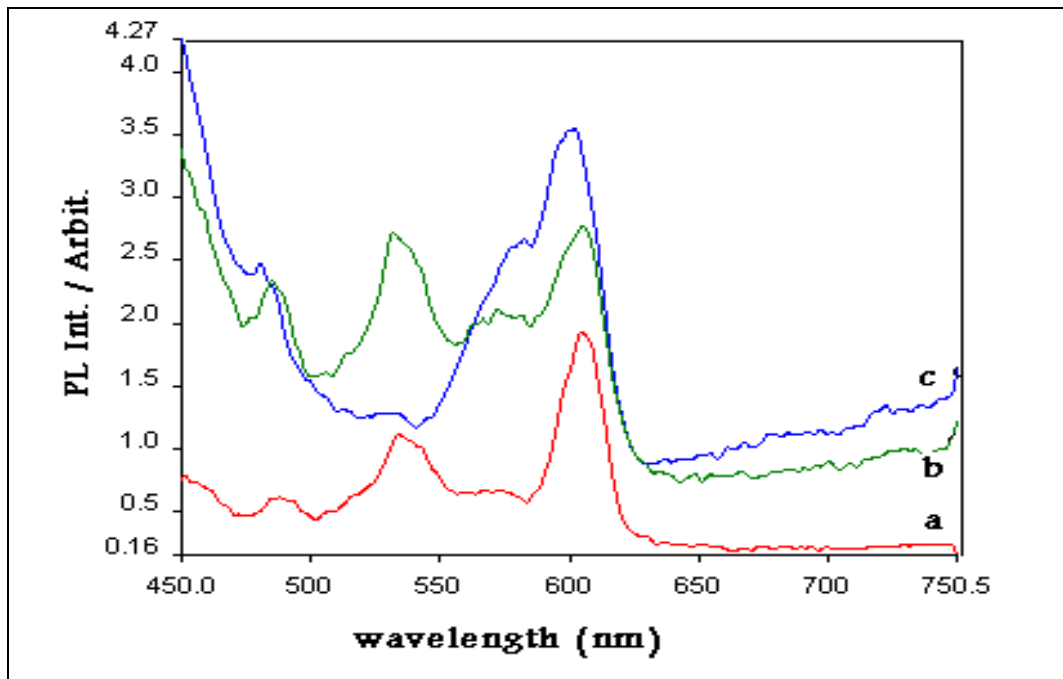
Figure (3.11): Photo-Luminescence Spectra for CdS/FTO/Glass film, a) before annealing, b) after annealing, and c) for FTO/Glass substrate.

The value for PL emission wavelength coincided with the value for electronic absorption spectra of CBD-CdS films. Figure (3.12) shows the electronic absorption spectra for non annealed CdS thin films with absorption edge of ~535 nm, and the band gap was ~ 2.31 eV. This material contains interband transitions thus the absorption coefficient does not go to zero even for long wavelength incident light.
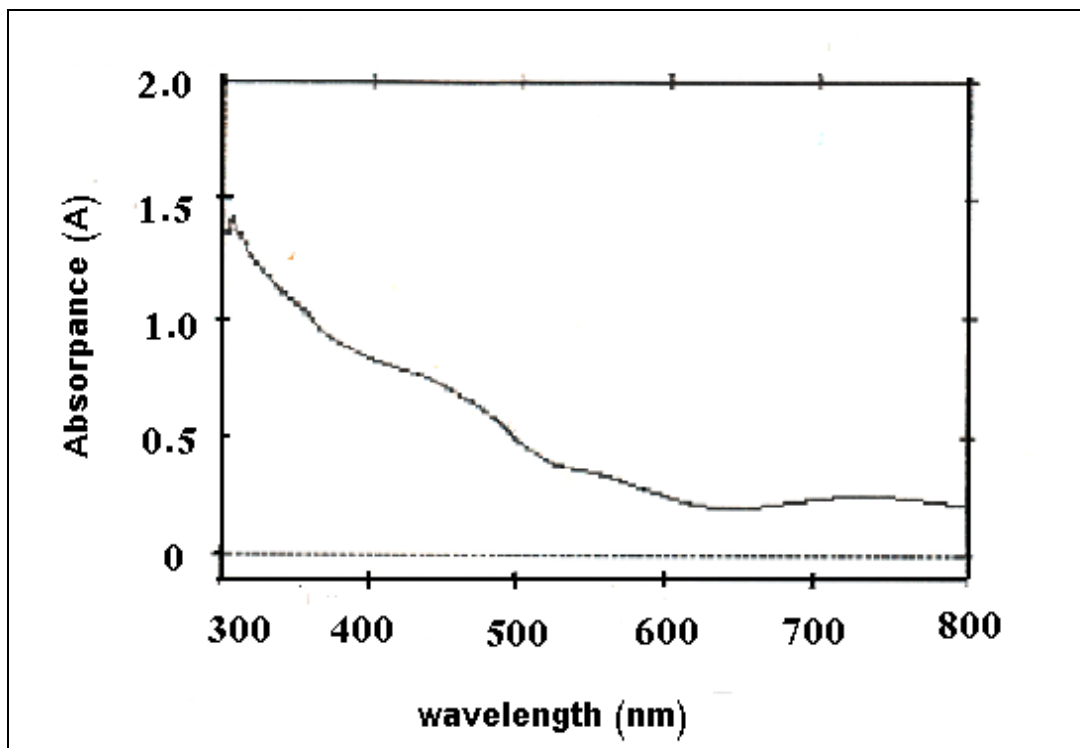
Figure (3.12): Electronic Absorption Spectra for non- annealed CBD-CdS films.

3.3.4 Dark *J-V* Plots of CdS Thin Film Electrodes

Dark *J-V* plots of CBD-CdS films showed no significant enhancement in *J-V* plots for CBD-CdS film electrodes by annealing & slow cooling process. Thus the dark *J-V* plot of non-annealed CdS film electrode showed nearly same V_{onset} for the annealed CBD-CdS film electrode, Figure (3.13).
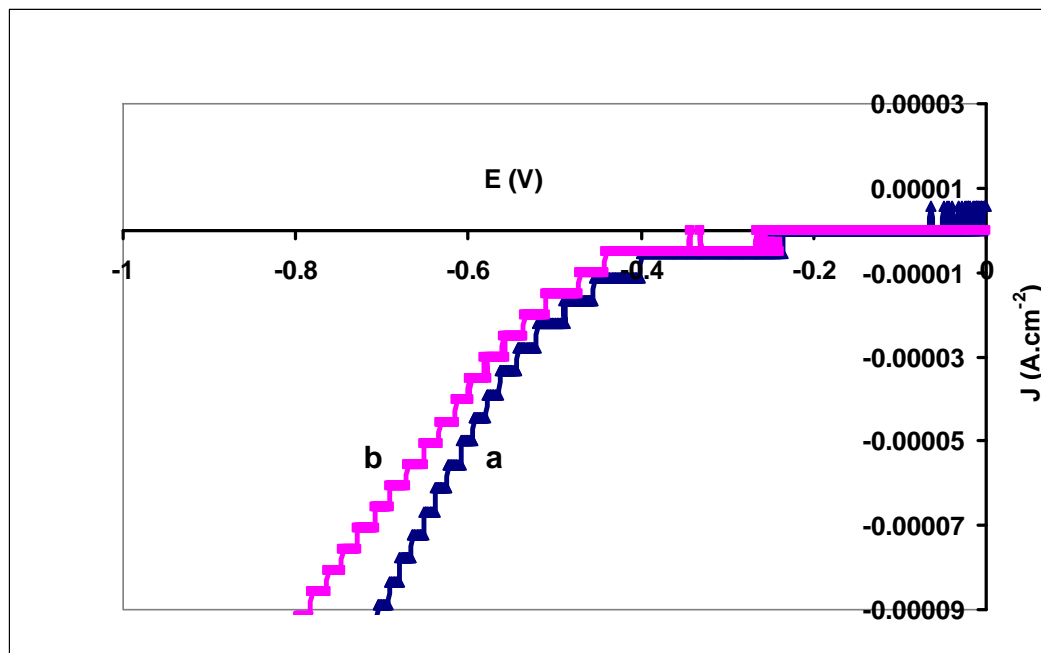
Figure (3.13): Dark *J-V* Plots for CBD-CdS film a) before annealing, b) after annealing & slow cooling. All *J-V* measurements were conducted in aqueous S^{2-} /S_x^{2-} redox system at room temperature.

3.3.5 Photo *J-V* Plots of CdS Thin Film Electrodes

For nano-sized CdS particles prepared by CBD technique, annealed & slow cooled CdS thin films showed better *J-V* plots than non annealed counterparts, Figure (3.14). Annealed & slow cooled CBD-CdS films showed higher J_{sc}, V_{oc} than non-annealed, and consequently gave percentage conversion efficiency (η % ~0.215) higher than non-annealed CBD-CdS film counterparts (η % ~0.11). Differences in photo *J-V* plots for annealed and non-annealed electrodes are consistent with SEM and XRD measurements shown earlier.
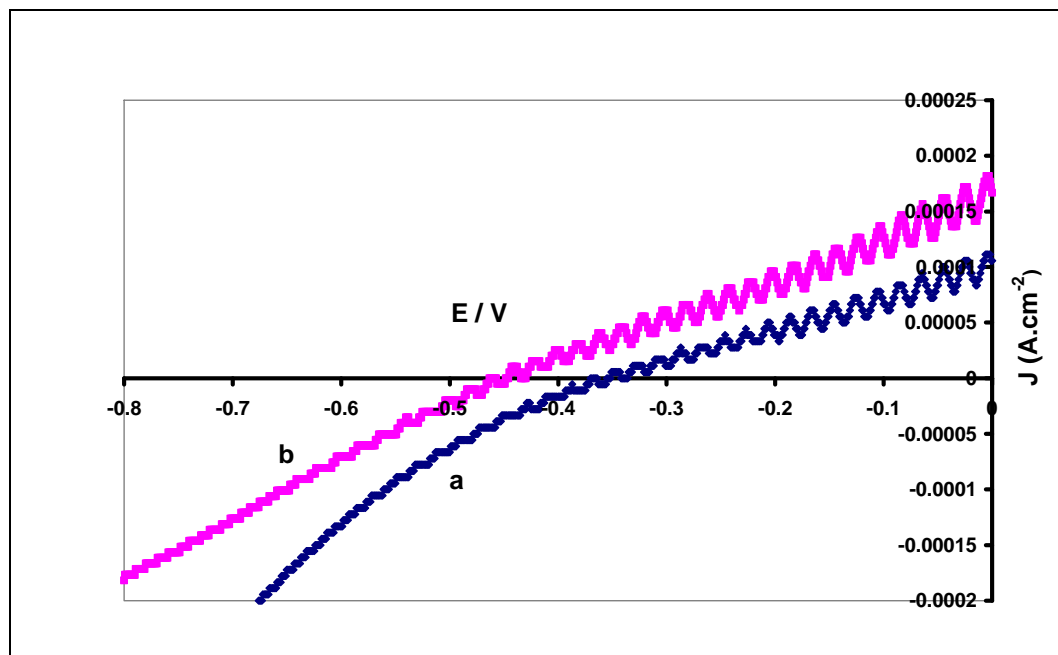
Figure (3.14): Photo *J-V* Plots for CBD-CdS film, a) before annealing, b) after annealing & slow cooling. All measurements were conducted in aqueous S^{2-}/S_x^{2-} redox system at room temperature.

3.3.6 Effect of CBD-CdS Film Annealing on Electrode Stability

The stability of different CBD-CdS thin films, annealed and non-annealed, under PEC conditions has been studied. The value of J_{sc} vs. time was measured using 0.0V applied potential (*vs.* SCE). The effect of annealing & slow cooling on J_{sc} vs. time plots has been studied.

It is found that annealed & slow cooled CdS films showed higher J_{sc} than non-annealed CdS film counterpart with almost a steady value for more than 150 min. This indicates the relative stability of annealed CdS thin films under PEC conditions, Figure (3.15).
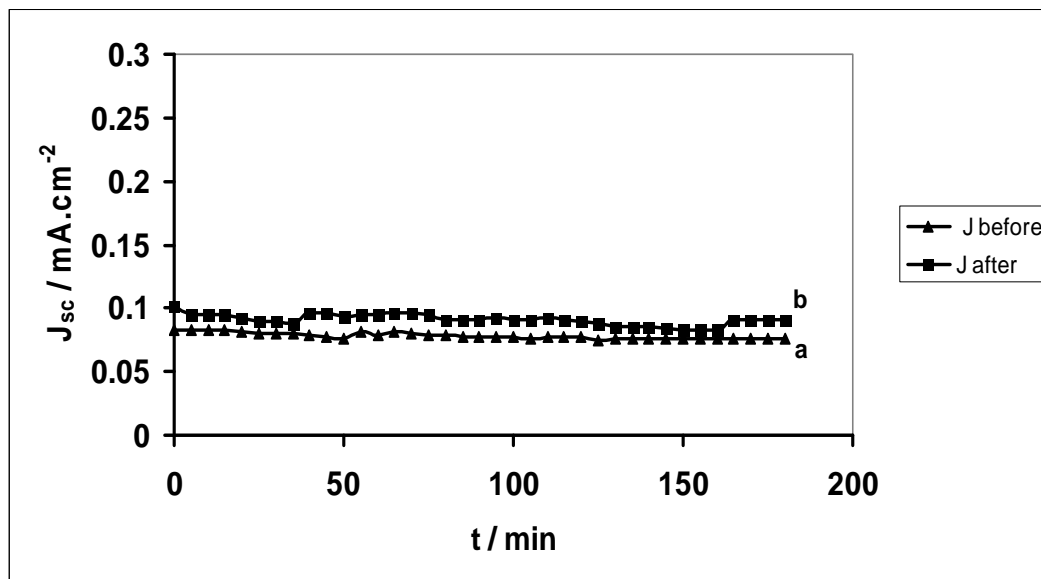
Figure (3.15): short circuit current density vs. time measured for CBD-CdS thin film electrodes, a) before annealing, b) after annealing & slow cooling. All measurements were conducted in aqueous S^{2-}/S_x^{2-} redox system at room temperature.

3.4 Electrochemical/Chemical Bath Deposited (EC/CBD) Electrodes

3.4.1 XRD Spectra for CdS Thin Film Electrodes

XRD measurements were obtained for both annealed and non-annealed EC/CBD-CdS films. XRD data showed that there was more crystallization and more orientation for both cases of EC/CBD-CdS films. X-ray diffraction patterns are shown in Figure (3.16) and Table (3.3). The average grain size of the CdS was estimated using Debye-Scherrers' formula. The average grain size for CdS nano-particles was found to be ~45 nm before annealing, and increased to ~55 nm after annealing & slow cooling. Figure (3.16 a,b) summarizes these these observations. The film involved both cubic and hexagonal phases with no change in crystalline structure of EC/CBD-CdS films after heat treatment under N_2 atmosphere.
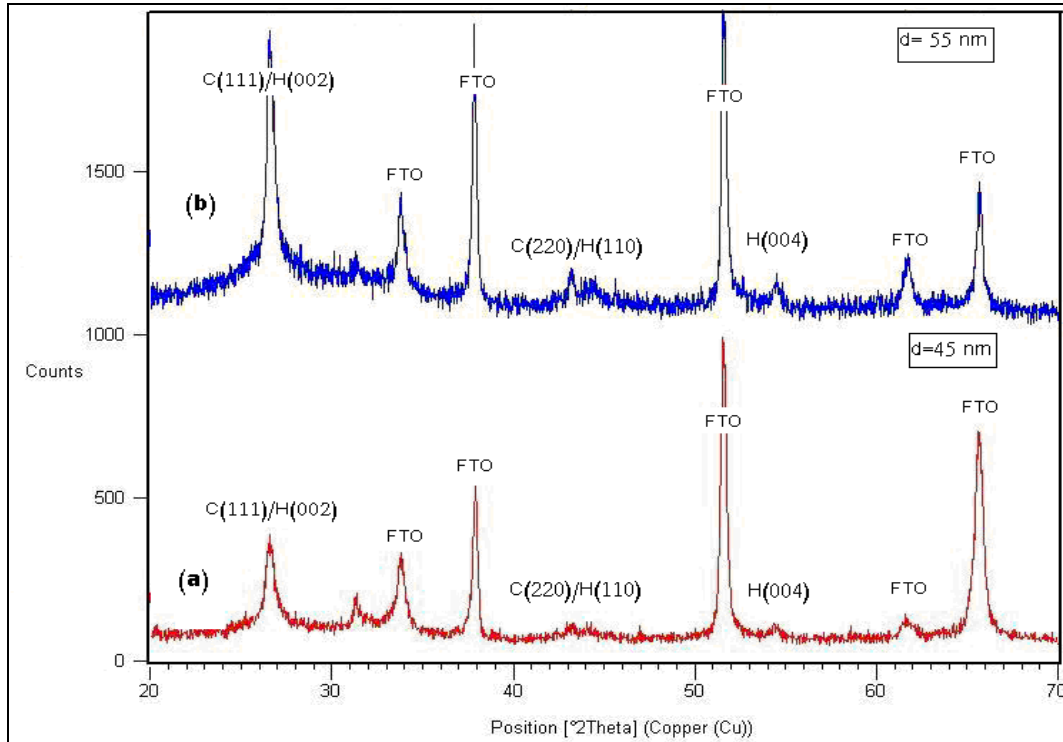
Figure (3.16): X-ray diffraction of EC/CBD-CdS film, a) before annealing, and b) after annealing & slow cooling.

Table (3.3): XRD measurements for EC/CBD-CdS films before and after annealing.

Position of observed peak (2 theta)	Cubic (C) (h k l)	Hexagonal(H) (h k l)	References
(non-annealed) 26.53	C(111)	H (002)	[61]
33.80	FTO subs.	----	[62]
37.93	FTO subs.	----	[62]
43.16	C(220)	H(110)	[61]
51.55	FTO subs.	----	[62]
54.43	H (004)	----	[61]
61.59	FTO subs.	----	[62]
65.59	FTO subs.	----	[62]
(Annealed) 26.52	C(111)	H (002)	[61]
33.81	FTO subs.	----	[62]
37.82	FTO subs.	----	[62]
43.22	C(220)	H(110)	[61]
51.54	FTO subs.	----	[62]
54.47	H (004)	----	[61]
61.66	FTO subs.	----	[62]
65.63	FTO subs.	----	[62]

3.4.2 SEM Images for EC/CBD Films

SEM surface images were obtained for EC/CBD-CdS thin films before and after annealing & slow cooling. Comparison between SEM images for annealed and non-annealed EC/CBD-CdS electrodes, showed that the latter had non-uniform and separate distinct layers of EC and CBD. The non-annealed films also showed smaller nano-particles (45 nm) than the annealed film (57 nm), Figure (3.17a). The coagulates present in the non-annealed film are less ordered and non-uniformly packed than annealed electrode. Annealing & slow cooling enhanced the SEM images and produced more homogeneous layers with more uniform coagulates, Figure (3.17b).
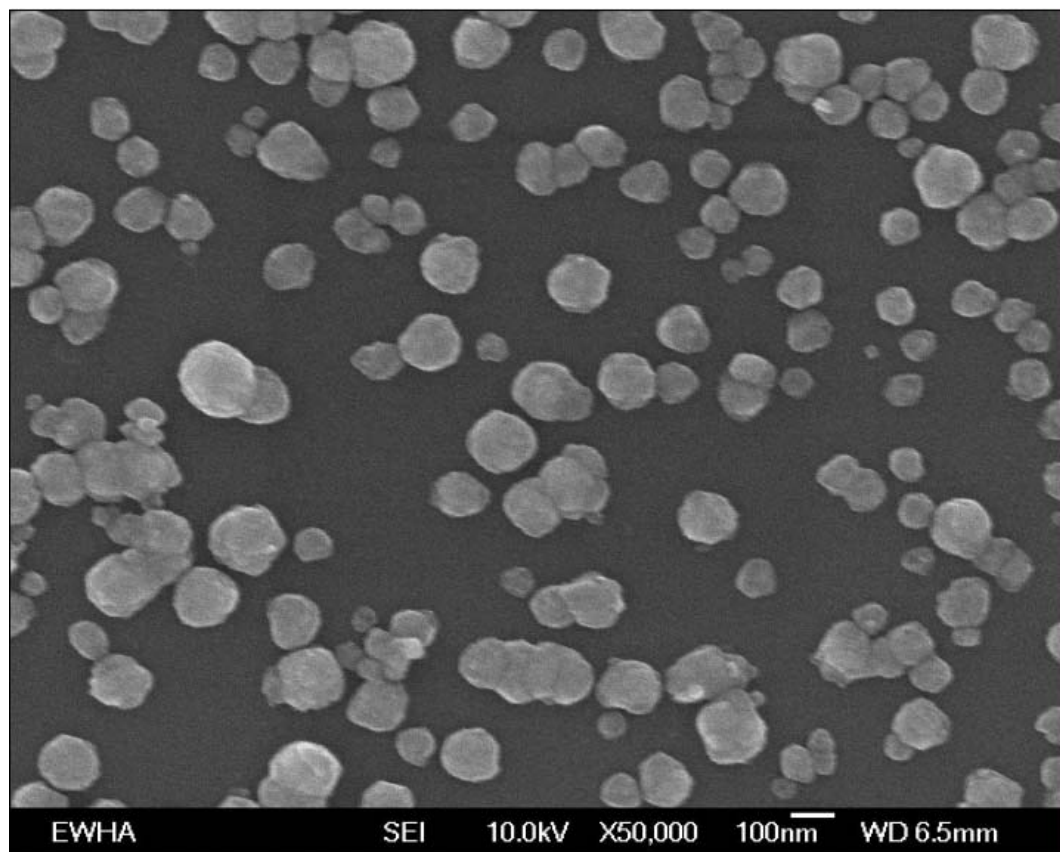
Figure (3.17a): SEM surface for EC/CBD-CdS thin film before annealing.
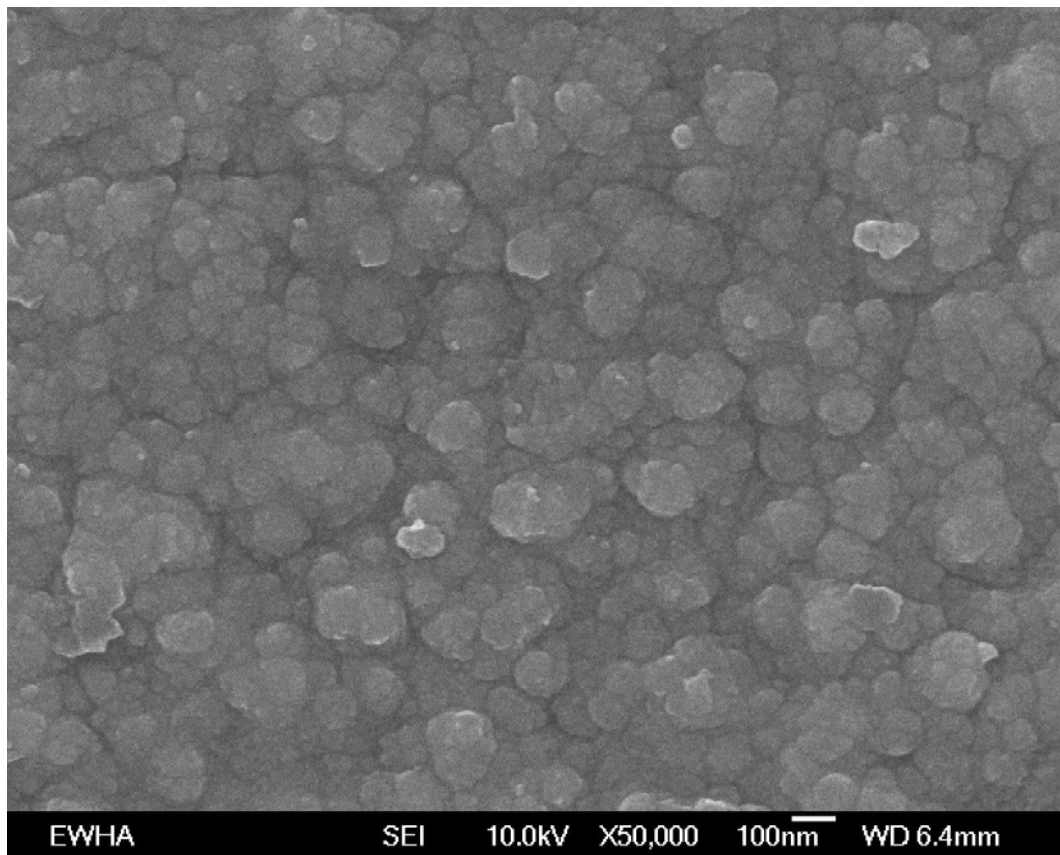
Figure (3.17b): SEM surface for EC/CBD-CdS thin film after annealing & slow cooling.

3.4.3 Photoluminescence Spectra

Photoluminescence spectra for EC/CBD-CdS films were investigated before and after annealing & slow cooling. Similar patterns were observed for photoluminescence spectra of films before and after annealing. Highest emission intensities appeared at wavelength ~535.7 nm, showing a band gap 1240/535.7 = 2.31 eV.

Photoluminescence intensity of untreated EC/CBD-CdS films had lower maximum intensity value (~1.88 a.u) than annealed ones which showed maximum intensity value of (~3.5 a.u), Figures (3.18a-b). The additional wavelength at wavelength ~600 nm, was due to FTO/Glass

substrate. The intensity for FTO in non-annealed EC/CBD film was ~1.68 (a.u), and with the annealed electrode it showed lower value (~1.25 a.u), Figure (3.18).
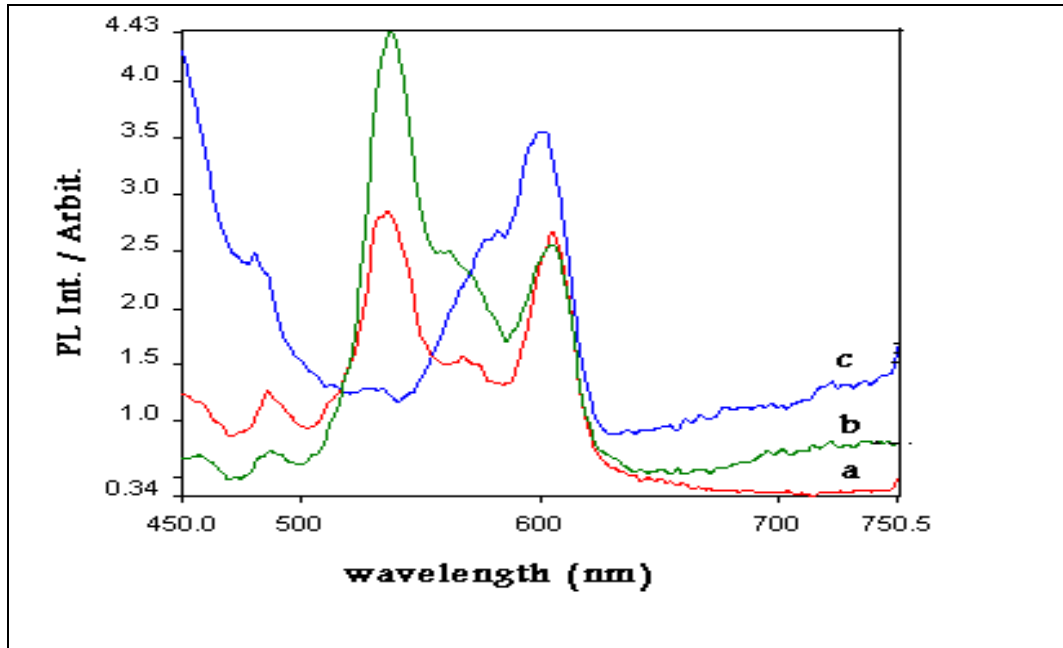
Figure (3.18): Photo-Luminescence Spectra for CdS/FTO/Glass film, a) before annealing, b) after annealing, and c) for FTO/Glass substrate.

The value for PL emission wave-length coincided with the value for electronic absorption spectra of EC/CBD-CdS films. Figure (3.19) shows the electronic absorption spectra for non annealed CdS thin films with good absorption edge of ~535 nm, and 2.31 eV band gap.
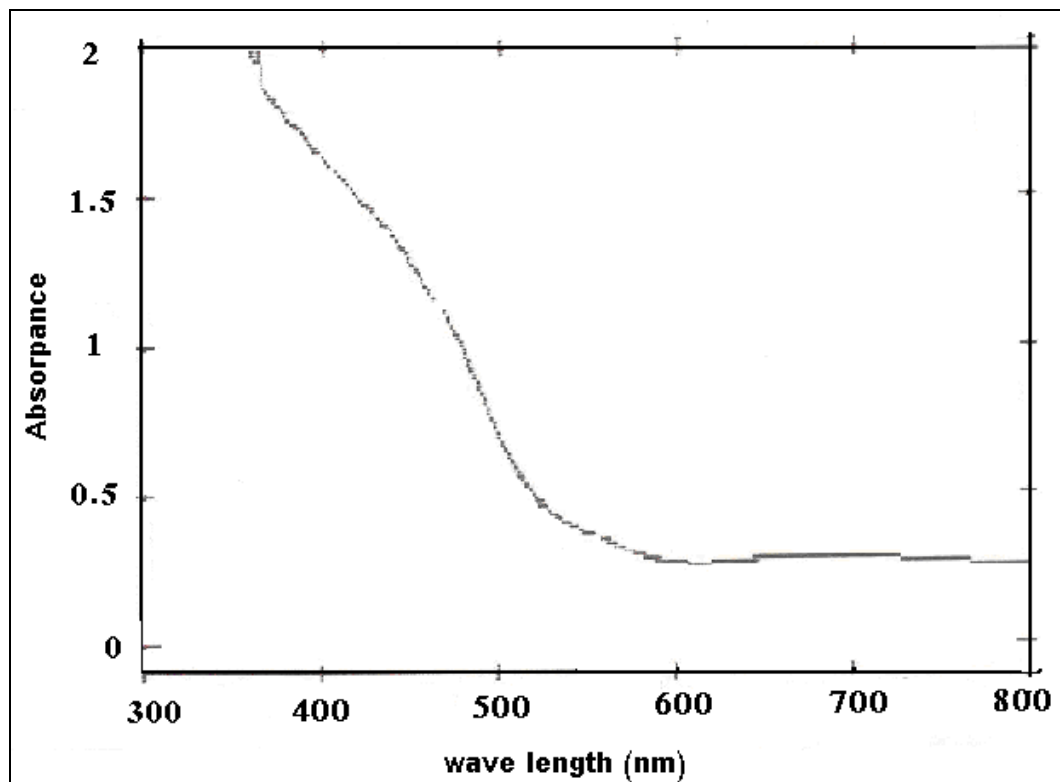
Figure (3.19): Electronic Absorption Spectra for non- annealed EC/CBD-CdS films.

3.4.4 Dark *J-V* Plots of CdS Thin Film Electrodes

Dark *J-V* plots of EC/CBD-CdS films showed no enhancement by annealing & slow cooling. Thus the dark *J-V* plots of non-annealed CdS film electrode showed nearly similar V_{onset} to the annealed EC/CBD-CdS film electrode, Figure (3.20).
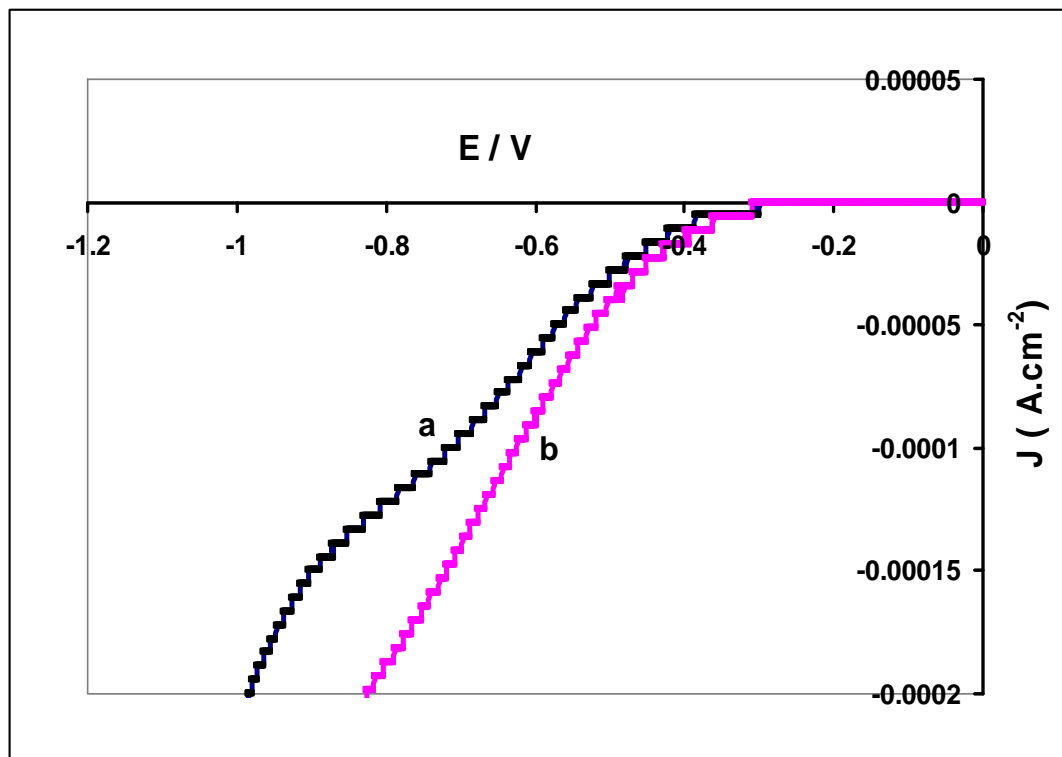
Figure (3.20): Dark *J-V* Plots for EC/CBD-CdS film a) before annealing, b) after annealing & slow cooling. All *J-V* measurements were conducted in aqueous S^{2-}/S$_x^{2-}$ redox system at room temperature.

3.4.5 Photo *J-V* Plots of CdS Thin Film Electrodes

Annealed & slow cooled EC/CBD-CdS thin films showed better *J-V* plots than non annealed counterparts, Figure (3.21). Annealed & slow cooled EC/CBD-CdS films showed higher *J$_{sc}$*, *V$_{oc}$*, and consequently showed higher percentage conversion efficiency (η%) than non-annealed counterparts. While the annealed films showed η % ~0.237%, the non-annealed electrodes showed only ~0.06%. Differences in photo *J-V* plots for annealed and non-annealed electrodes are consistent with SEM and XRD measurements shown earlier.
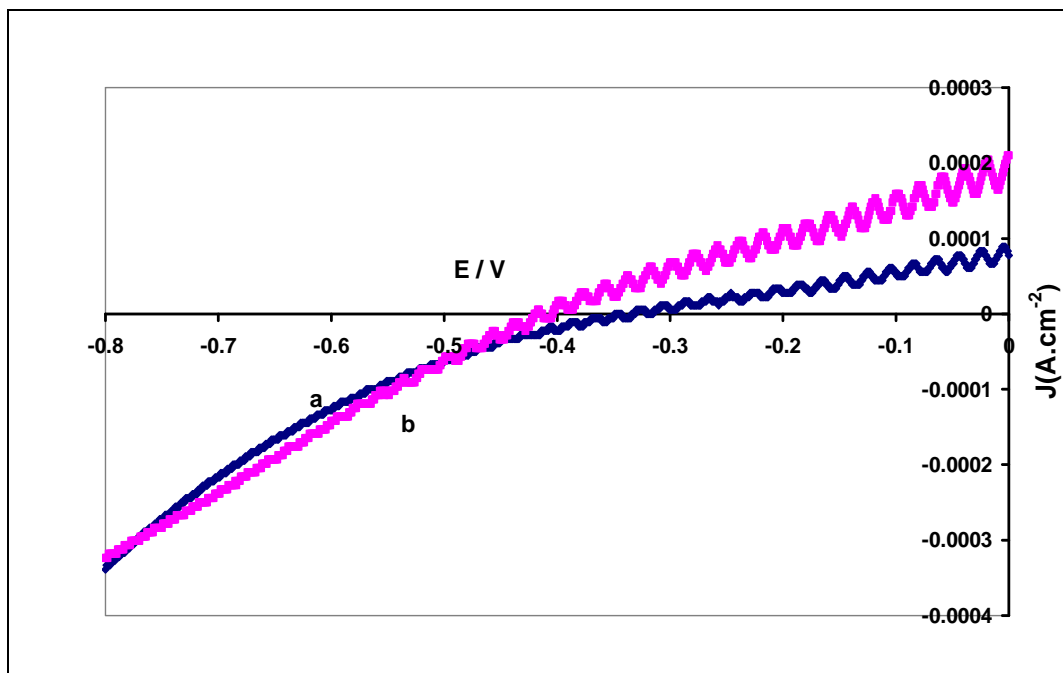
Figure (3.21): Photo _J-V_ Plots for EC/CBD-CdS film, a) before annealing, b) after annealing & slow cooling. All measurements were conducted in aqueous S^{2-}/S_x^{2-} redox system at room temperature.

3.4.6 Effect of Annealing on EC/CBD-CdS Electrode Stability

Effect of annealing on film stability has been studied under illumination. Plots of J_{sc} vs. time were measured for non-annealed and pre-heated electrodes. Figure (3.22) summarizes these findings. It was found that annealed & slow cooled CdS films showed higher J_{sc} than non-annealed CdS film counterpart, for three hours. This indicates that J_{sc} values can be improved by annealing and slow cooling process and may give good stability for a certain period of time.
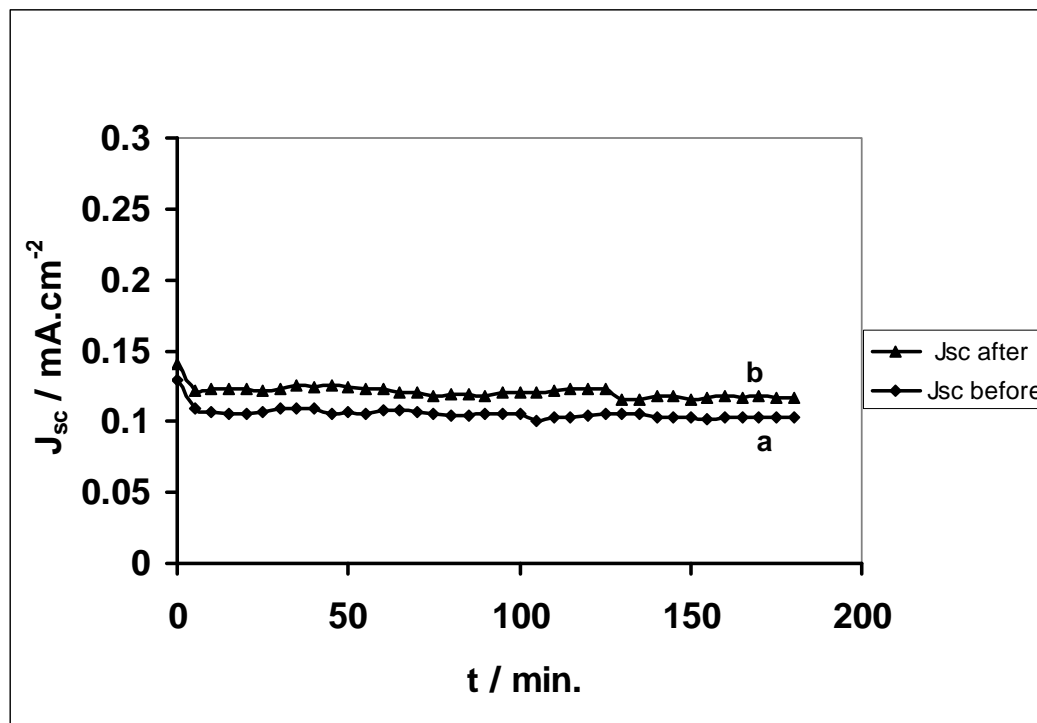
Figure (3.22): short circuit current density vs. time measured for EC/CBD-CdS thin film electrodes, a) before annealing, b) after annealing & slow cooling. All measurements were conducted in aqueous S^{2-}/S_x^{2-} redox system at room temperature.

Chapter Four

Discussion

Chapter Four
Discussion

4.1 General Remarks

Annealing of SC's was reported to enhance the crystals homogeneity, quality, performance, and structure. Annealing also reduces defects, removes surface roughness and consequently enhances SC characteristics [52-60].

Slow cooling was also reported to enhance SC characteristics [63-69]. Slow cooling causes uniform contraction for annealed SC and improves its crystallinity. Moreover, slowly cooled crystals may retain their original order.

In this work, we investigated such ideas to improve PEC characteristics of CdS thin films. Moreover, we utilized a new technique (EC/CBD) to achieve this purpose. To our knowledge, such technique has not been utilized as a technique to enhance PEC characteristics of CdS film SC's.

In this chapter, we discuss the obtained results, revealing the advantages of combined EC/CBD preparation, annealing and slow cooling on SEM surface images, XRD patterns, electronic absorption spectra, PL spectra and *J-V* plots.

4.2 Effect of Annealing on XRD Spectra

A comparison between XRD spectra for different CdS films before and after annealing was studied. Annealing lowered the crystallite size for

EC-CdS films which have comparable intensities with preferential orientation in the C(220)/H(110), C(111)/H(002) and H(004) directions, Figure (3.3). This is acceptable as the EC-CdS are expected to be relatively uniform and crystalline even before annealing. Thus heating may increase their disorder and yield smaller particle size.

On the other hand, annealing enhanced the crystallite size in both CBD-CdS and EC/CBD-CdS films. The crystallite size was enhanced from 31 nm to 41 nm in CBD process, and from 45 nm to 55 nm in EC/CBD, Figures (3.9 and 3.16) respectively. The increase in crystallite sizes for EC/CBD-CdS and CBD-CdS particles is due to lowering of disorder in the crystallites, as observed in literature [52-60].

The enhancement in crystallite size was accompanied with enhancement in the Photo-electrochemical conversion efficiency. This is because annealing decreases cracks, defects and disorders that may exist in the CdS crystallites [69-71]. This consequently makes electrons easy to transfer inside the particle and between adjacent particles, of the CdS film, as well. EC/CBD-CdS films have preferential orientation in the C(220)/H(110), C(111)/H(002) and H(004) directions, and CBD-CdS films have preferential orientation in the C(111)/H(002) and H(004) directions.

4.3 Effect of Annealing on SEM Images

CdS thin films were deposited onto FTO/Glass substrates by EC, CBD and EC/CBD techniques. Comparison between SEM images for

different un-treated CdS films was investigated. SEM images of CBD-CdS films showed small nano-sized particles, nearly spherical shaped coagulates with cracks, Figure (3.10a). In addition, CBD-CdS film images showed more uniform surface compared to EC/CBD-CdS film images which showed non homogeneous and separate distinct layers of EC and CBD, Figure (3.17a). SEM images also showed that un-treated EC/CBD-CdS films had larger nano-particles (~45 nm in diameter) than CBD-CdS films (~35 nm).

All deposited films were modified by annealing & gradual slow cooling process. Annealing enhanced the SEM images for different CdS films. This is consistent with other works [72-73]. Both annealed CBD-CdS and EC/CBD-CdS film images showed soundly homogenized layers with more ordered and uniformly packed nearly spherical shaped coagulates than EC-CdS film, Figures (3.10b, 3.17b, 3.4b) respectively.

SEM images for treated EC-CdS films showed ups and downs in surface (with nano-particles ~35 nm), indicating relatively lower uniformity surface than other counterparts. This is because annealing may increase their disorder and yield smaller particle size, Figure (3.4).

4.4 Effect of Annealing on PL Spectra

Photoluminescence spectra for different CdS films were investigated before and after annealing. PL spectra for EC/CBD-CdS, CBD-CdS, and EC-CdS films showed similar emission wavelengths before and after

annealing. Highest emission intensities appeared at around 535 nm and the band gap was ~2.3 eV for all systems, Figures (3.18a-b, 3.11a-b, 3.5a-b). On the other hand, PL intensity values for both non-annealed EC/CBD-CdS (1.88 a.u) and CBD-CdS (0.625 a.u) films were lower than those for the annealed counterparts (3.5, 1.1 a.u respectively). This is because annealing enhances the particle characteristics, giving more uniform, and compact surface and consequently higher PL intensity. This is consistent with other works [74- 75].

In addition, PL intensity value for annealed EC-CdS electrode (1.7 a.u) was higher than that for non-annealed counterpart (1.4 a.u). This indicates that annealing enhanced the characteristics inside nano-particles, and enhanced the contact between adjacent CdS nano-particles, and hence, enhanced PL intensity.

The PL intensity value for non-annealed EC/CBD-CdS film was higher than that for both non-annealed EC-CdS and CBD-CdS counterparts. This may be attributed to the fact that EC/CBD-CdS consists of two distinct layers with higher thickness than CBD-CdS and EC-CdS films.

Moreover, The PL intensity value for annealed EC/CBD-CdS film was higher than that for both annealed EC-CdS and CBD-CdS counterparts. This may be attributed to the fact that EC/CBD-CdS film has higher thickness than its counterparts (EC & CBD). The film also exhibited

homogenized layers with more ordered and uniformly packed coagulates than either EC or CBD-CdS films.

All films showed an emission band corresponding to FTO with maximum wavelength approximately at 600 nm. The intensity value for FTO emission varied with different films. It was ~1.3 (a.u) for annealed CBD-CdS, ~5 (a.u) for annealed EC-CdS, and ~1.25 (a.u) for annealed EC/CBD-CdS. The EC-CdS film exhibited highest FTO emission intensity. This is may be because EC-CdS film is very thin and allows incident wavelength ($\lambda_{excitation}$) to penetrate CdS film to FTO/Glass substrate.

The value for PL emission spectra coincided with the value for electronic absorption spectra of both CBD-CdS and EC/CBD-CdS films, Figs. (3.12, 3.19). Electronic absorption spectra for non-annealed EC/CBD-CdS film showed sharper absorption edge than CBD-CdS film, at ~535 nm. This indicates that EC/CBD-CdS film had better and more defined absorption spectra. In case of EC-CdS film, electronic absorption spectrum was difficult to measure due to the very thin film of CdS.

4.5 Effect of Annealing on Dark *J-V* Plots

It is known that annealing should give better dark *J-V* plots than non-annealed process counterpart [72]. Annealing process will reduce the crystal defects, surface roughness, and hence, will improve the crystallinity, and then would give better dark *J-V* plots with better V_{onset}. Moreover, surface roughness and crystal disorder inhibit dark current occurrence. We

can explain that as follows: with higher surface crystal roughness or disorder, the surface states are dominant. Such surface states would inhibit the majority carrier transfer across the SC/liquid interface. This inhibition will lower the dark current density. Annealing reduces the surface states density by improving SC crystallinity, and consequently enhances dark current density [72, 76].

In this study, it was found that dark J-V plots showed the same patterns for different CdS films before and after annealing. Figure (3.6) showed that annealed EC-CdS film exhibited similar dark J-V plots to non-annealed electrode (with V_{onset} -0.3 V). Similar result was observed for EC/CBD-CdS (V_{onset} -0.3 V) films. On the other hand, the CBD-CdS showed different V_{onset} value (-0.24 V), Figures (3.20, 3.13) summarized these observations. This is presumably due to the very thin film thickness, due to the annealing temperature (250^0C) being not high enough to affect characteristics.

4.6 Effect of Annealing on Photo *J-V* Plots & Conversion Efficiency

In general, annealing CdS thin films improves the photo J-V plots [36, 77]. In this study, annealed & slow cooled EC/CBD-CdS thin films showed better J-V plots than non-annealed counterpart, Figure (3.21). Photo J-V plots for both EC-CdS and CBD-CdS films showed similar results, Figures (3.7, 3.14). Similarly, preheating enhanced CdS film conversion efficiency. Annealed films showed better conversion efficiency and higher fill factor (FF) than non-annealed films, Table (4.1).

Enhancement of conversion efficiency and FF were due to the short-circuit current density and open circuit voltage enhancement, as discussed earlier.

Moreover, annealed EC-CdS electrode exhibited higher conversion efficiency than non-annealed electrode. This is possibly because annealing enhanced the contact between adjacent CdS nano-particles, despite the low uniformity surface of CdS as shown in SEM topography. Moreover, annealing enhanced the characteristics inside nano-particle itself as observed from PL intensity. Annealing decreased the defects inside the particles. This is consistent with literature reports [69-71].

On the other hand, the high conversion efficiency of both annealed CBD-CdS and EC/CBD-CdS films, compared to non-annealed counterparts, coincided with SEM topography, XRD spectra and PL intensity results. This is consistent with literature [78]. XRD patterns showed enhancement in crystallite size for both annealed CBD-CdS and EC/CBD-CdS films. SEM images showed homogenized layers with more ordered and uniformly packed coagulates for annealed films. In addition, PL specra for annealed films exhibited higher emission values than non-annealed films. This is because annealing enhances the particle characteristics, giving more uniform, and compact surface and consequently higher PL intensity. This is consistent with literature reports [69-71].

Table (4.1): Effect of annealing & slow cooling of different CdS films on PEC characteristics.

Type of deposition	J_{sc} (A.cm^{-2})	V_{oc} (V)	η (%)[a]	FF (%)[b]
EC (non-annealed)	5 x 10^{-5}	-0.307	0.043	24.3
(annealed)	1 x 10^{-4}	-0.33	0.103	27.06
CBD (non-annealed)	1 x 10^{-4}	-0.34	0.11	22.7
(annealed)	1.7 x10^{-4}	-0.44	0.215	24.7
EC/CBD(non-annealed)	8.33 x 10^{-5}	-0.318	0.06	21.9
(annealed)	1.88 x 10^{-4}	-0.41	0.237	26.3

[a]η (%) = [(maximum observed power density)/(reach-in power density)]×100%.

[b]FF = [(maximum observed power density)/$J_{SC} \times V_{OC}$]×100%.

Non-annealed CBD-CdS films showed better photo *J-V* plots and higher conversion efficiency than either EC-CdS or EC/CBD-CdS non-annealed films, Figure (4.1). Contrary to that, annealed EC/CBD-CdS films showed better photo *J-V* plots and higher conversion efficiency than either EC-CdS or CBD-CdS annealed films, Figure (4.2).
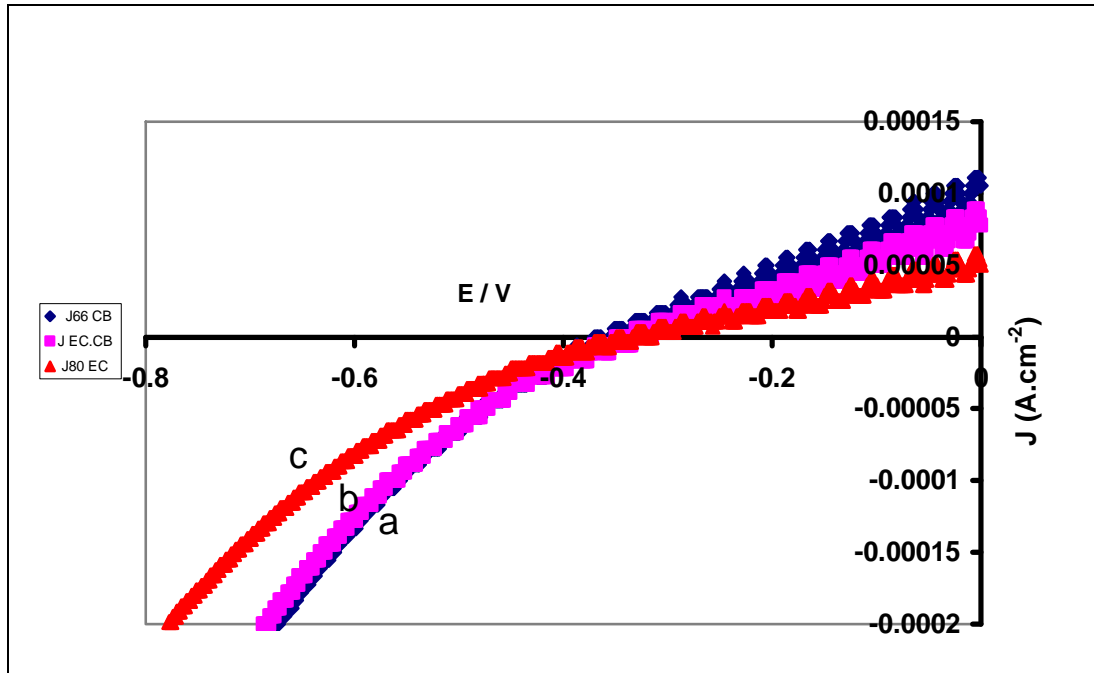
Figure (4.1): Photo *J-V* plots of different CdS films before annealing, a) CBD-CdS, b) EC/CBD-CdS, c) EC-CdS. All measurements were conducted in aqueous S^{2-}/S$_x^{2-}$ redox system at room temperature.
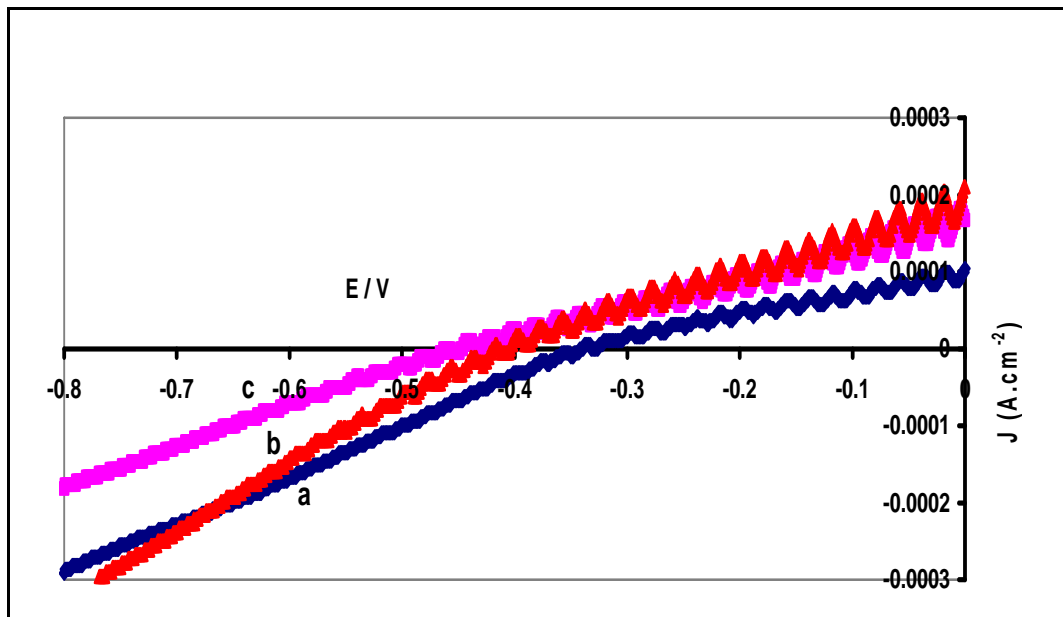
Figure (4.2): Photo *J-V* plots of different CdS films after annealing & slow cooling, a) EC-CdS, b) EC/CBD-CdS, c) CBD-CdS. All measurements were conducted in aqueous S^{2-}/S_x^{2-} redox system at room temperature.

4.7 Effect of Annealing on Stability

In this work, effect of annealing on CdS film stability under PEC conditions had been studied. Plots of J_{sc} vs. time were measured for different CdS films, before and after annealing. Figure (3.8) showed that the J_{sc} value had been improved for annealed & slowly cooled EC-CdS electrode at $250^{o}C$ for as long as 150 minutes. After that, J_{sc} value went down and coincided with non-annealed electrode J_{sc} value. It can be concluded that there was no much difference between stabilities of annealed and non-annealed EC-CdS electrodes.

Figures (3.15, 3.22) showed that annealed & slow cooled CBD-CdS and EC/CBD-CdS electrodes exhibited higher J_{sc} than non-annealed CdS films counterparts for about three hours. That is because, annealing

increases the grain size of nano-particles, removes defects and consequently, enhances the film surface and improves the stability. Moreover, annealing enhances minority carrier diffusion to electrolyte solution in PEC cell, which prevents electrode photo-corrosion normally associated with hole accumulation in the SCL [79]. Figures (4.3, 4.4) showed similar patterns for both annealed and non-annealed CdS films, prepared by different techniques. In both cases, CBD-CdS films showed higher J_{sc} vs. time plot than EC-CdS film, but lower than EC/CBD-CdS film for as long as 150 minutes. In contrary, there was conflict with photo J-V plots of non-annealed CBD-CdS and EC/CBD-CdS films results as mentioned earlier. Therefore, stability results were considered, due to measurable J_{sc} for pro-longed time.
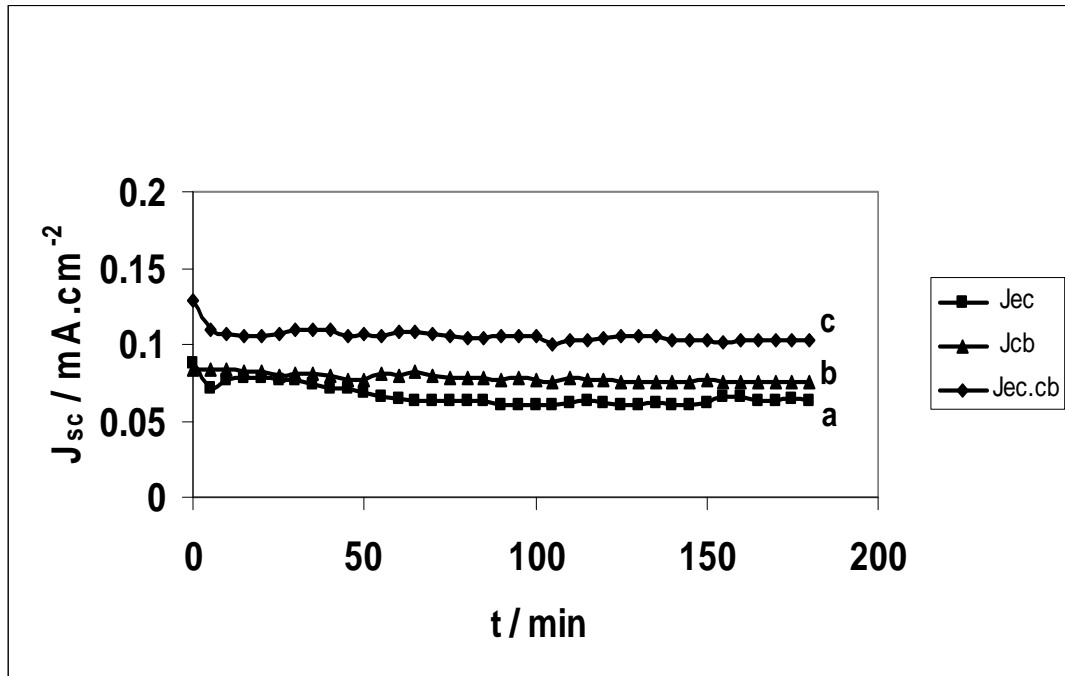
Figure (4.3): short circuit current density vs. time measured for non-annealed a) EC-CdS, b) CBD-CdS, and c) EC/CBD-CdS electrodes. All measurements were conducted in aqueous S^{2-}/S_x^{2-} redox system at room temperature.
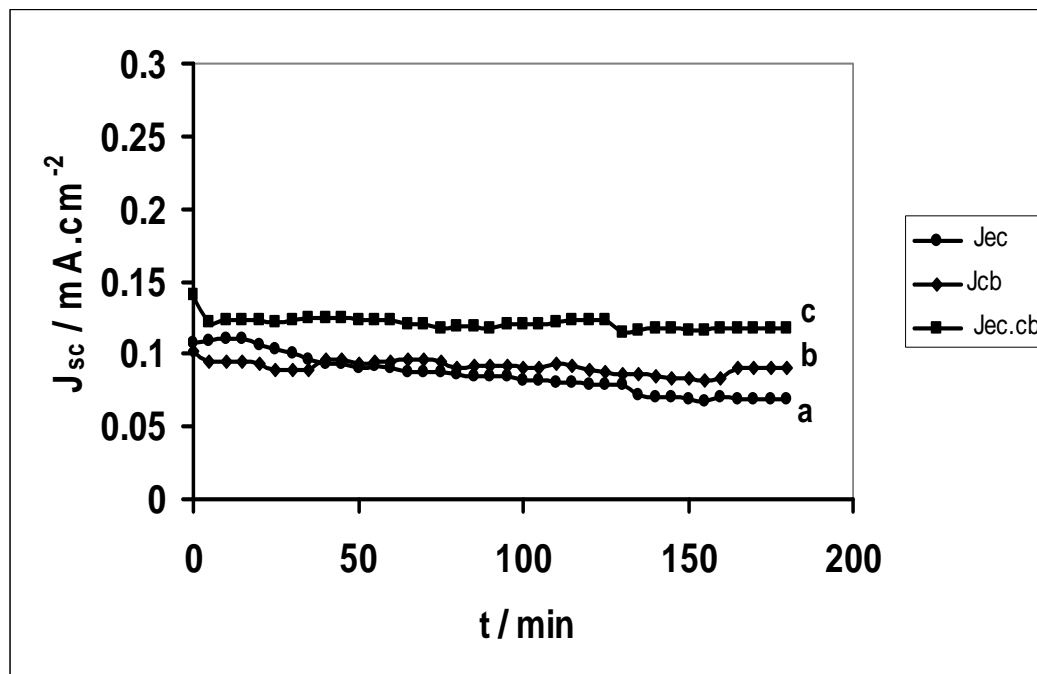
Figure (4.4): short circuit current density vs. time measured for annealed & slow cooled a) EC-CdS, b) CBD-CdS, and c) EC/CBD-CdS electrodes. All measurements were conducted in aqueous S^{2-}/S_x^{2-} redox system at room temperature.

Conclusions

- CdS thin films were prepared by three different techniques, including EC, CBD, EC/CBD techniques. All films showed PEC behaviors.

- CBD-CdS thin films showed higher efficiency in PEC systems than its EC/CBD-CdS and EC-CdS films counterparts.

- Annealing & slow cooling process showed enhancement in PEC cell efficiency for different CdS thin film electrodes.

- Annealed EC/CBD-CdS thin film showed higher conversion efficiency in PEC systems than its counterparts.

- EC/CBD films showed higher values of J_{sc} vs. time than either EC or CBD counterparts.

- Annealing & slow cooling process affected characteristics of different prepared CdS thin films, such as, SEM, XRD spectra.

- Enhancement of efficiency and stability of different CdS films coincided with enhancements in XRD and SEM characteristics of the films.

- Similar patterns were observed for PL spectra of different CdS thin film electrodes.

Suggestions for Further Work

For future work, we recommend doing the following:

1) Prepare CdS thin films using different techniques such as: EC, CBD, EC/CBD, with multi deposition processes.

2) Use annealing with different temperatures to improve the PEC characteristics.

3) Study the effect of cooling rates (such as slow cooling and quenching) of different annealed films, at different temperatures, on PEC characteristics.

4) Modify the CdS films with coating material such as electroactive polymers.

5) Apply different PEC cells using different experimental conditions and different redox couples to enhance electrode efficiency and stability.

References

[1] J. A. Turner, "*A realizable renewable energy future*", **Science Magazine**, **285**, (1999), 687-689.

[2] http://ezinearticles.com/?The-importance-of-solar-energy-to-our-everyday-Lives&id=1909914, (date accessed, 16/2/2011).

[3] J. Bai, J. Li, Y. Liu, B. Zhou1, W. Cai, "*A new glass substrate photo-electrocatalytic electrode for efficient visible-light hydrogen production：CdS sensitized TiO2 nanotube arrays*", **Appl. Catal., B***, Volume **95**, (2010), Pages 408-413.

[4] http://esa21.kennesaw.edu/activities/solar/solaractivity.pdf, (date accessed, 16/2/2011).

[5] R. de Boer, "*Technologies and prospects for photochemical conversion and storage of solar energy: A survey of the state-of-the-art*", *ECN-C--01-029* ECN energy efficiency in industry (2001), pp. 7-9.

[6] C. Baird, "**Environmental chemistry**", 2nd ed., W. H. Freeman and Company, NY, (1999), pp. 251-251.

[7] http://www.ehow.com/how-does_4914210_why-solar-energy-important.html, (date accessed, 16/2/2011).

[8] Technical assessment analysis group (GCEP), "*An assessment of solar energy conversion technologies and research opportunities-technical report*", Stanford University, (2006), p. 13.

[9] A. R. West, "**Basic Solid State Chemistry**", 2nd ed., John Wiley and Sons, Chichester, (1994), pp. 299-300.

[10] L. Smart, and E. Moore, "**Solid State Chemistry**", 2nd ed., Chapman & Hall, London, (1992), pp. 87.

[11] M. Masoud, "**Surface modification of n-GaAs semiconductor with metalloporphyrin/polysiloxane matrices, effect of modification on: band-edge position, short circuit current and surface stability in aqueous photoelectrochemistry**", Master's Thesis, An-Najah National University, Nablus, Palestine, (2001) p. 4.

[12] See Ref.[5], p. 20.

[13] K. Rajeshwar, P. Singh, and J. DuBow, "*Energy conversion in photoelectrochemical systems-a review*", **Electrochem. Acta**, **23,** (1978), 11-17.

[14] S. N. SAHU and S. CHANDRA, "*Chemical bath deposited CdS and CdS:Li films and their use in photo-electrochemical solar cells*", **Sol. Cells**, **22**, (1987), 163 – 173.

[15] A. J. Nozik, "*Photoelectrochemistry: application to solar energy conversion*", **Ann. Rev. Phys. Chem.**, **29,** (1978), 189-222.

[16] B. Finnström, in **"Solar energy-photochemical processes available for energy conversion"**, Vol.14, eds. S. Claesson and B. Holmström, National Swedish Board for Energy Source Development, (1982), pp. 56-64.

[17] J. Koryta, J. Dvorak, and L. Karan, " **Principles of Electrochemistry**", 2nd ed., Chapman and Hall, Chichester, (1993), pp. 391-399.

[18] See Ref.[16], pp. 67-70.

[19] See Ref.[16], pp. 206-211.

[20] R. Ismail, " **Enhancement of photo-electrochemical characteristics of CdS thin film electrodes prepared by chemical bath deposition effect of annealing and rate of cooling**", Master's Thesis, An-Najah National University, Nablus, Palestine, (2008), p.4-7.

[21] H. O. Finklea, "**Semiconductor Electrode**", ed. H. O. Finklea, Elsevier, Amesterdam, (1988), pp. 18-22.

[22] See Ref. [20], p. 7

[23] **http://en.wikipedia.org/wiki/Semiconductor**, (date accessed, 26/3/2011).

[24] M. LoCascio, "*Application of semiconductor nanocrystals to photovoltaic energy conversion devices*", River Street, (2002), 1-12.

[25] S. Chandra, "**Photo-electochemical solar cell**", Gordon and Breach Science Publisher, New York, (1986), pp. 162-183.

[26] H. Jia, Y. Hu, Y. Tang, L. Zhang, *"Synthesis and photoelectrochemical behavior of nanocrystalline CdS film electrodes"*, **Electrochem. Commun**., **8,** (2006), 1381–1385.

[27] S. Soundeswaran, O. S. Kumar and R. Dhanasekaran, "*Effect of ammonium sulphate on chemical bath deposition of CdS thin films*", **Mater. Lett**., **58**, (2004), 2381–2385.

[28] J. P. Enríquez, X. Mathew, "*Influence of the thickness on structural, optical and electrical properties of chemical bath deposited CdS thin films*", **Sol. Energy Mater. Sol. Cells**, **76,** (2003), 313–322.

[29] B.O. Seraphin, "**Solar energy conversion-solid-state physics aspects**" vol. 31, ed. Springer-Verlag, New York, (1979) pp. 220-223.

[30] See Ref. [14], pp. 1.

[31] A.I. Oliva, R. Castro-Rodriguez, O. Solis-Canto, V. Sosa, P. Quintana, J.L. Pena," *Comparison of properties of CdS thin films grown by two techniques*", **Appl. Surf. Sci**., **205**, (2003), 56-64.

[32] B. N. Patil, D. B. Naikb , V. S. Shrivastava, "*Synthesis and characterization of Al doped CdS thin films grown by chemical bath deposition method and its application to remove dye by photocatalytic treatment*", **Chalcogenide Lett**., **8**, (2011), 117-121.

[33] J.N. Ximello-Quiebras, G. Contreras-Puente, J. Aguilar-Herna'ndez, G. Santana-Rodriguez, A. Arias-Carbajal Readigos, "*Physical properties of chemical bath deposited CdS thin films*", **Sol. Energy Mater. Sol. Cells**, **82**, (2004), 263–268.

[34] S. D. Sathaye and A. P. B. Sinha, "*Studies on thin films of cadmium sulphide prepared by a chemical deposition method*", **Thin Solid Films**, **37,** (1976), 15-23. .,

[35] J.M. Nel, H.L. Gaigher, F.D. Auret, "*Microstructures of electrodeposited CdS layers*", **Thin Solid Films**, **436**, (2003), 186–195.

[36] S. Chen, M. Paulose, C. Ruan, G. K. Mor, O. K. Varghese, D. Kouzoudis, C. A. Grimes, "*Electrochemically synthesized CdS nanoparticle-modified TiO_2 nanotube-array photoelectrodes: Preparation, characterization, and application to photoelectrochemical cells*", **J. Photochem. Photobiol. A**, **177**, (2006), 177–184.

[37] A. Mirmohseni, D. Farshbaf, M. Zarrabi, "*Electro deposition coating of epoxy resin on phosphated steel : Optimization of key factors*", **Int. J. of Polym. Mater**., **12,** (2004), 621-632.

[38] G. Sasikala, R. Dhanasekaran, C. Subramanian, "*Electrodeposition and optical characterization of CdS thin films on ITO-coated glass*", **Thin Solid Films**, **302,** (1997), 71-76.

[39] F. Kadirgan, D. Mao, W. Song, T. Ohno, B. Mccandles, "*Properties of electrodeposited cadmium sulfide films for photovoltaic devices with comparison to CdS films prepared by other methods*", **Turk J. Chem.**, **24,** (2000), 21- 33.

[40] S. Soundeswaran, O. Senthil Kumar, R. Dhanasekaran, "*Effect of ammonium sulphate on chemical bath deposition of CdS thin films*", **Mater. Lett**., **58**, (2004), 2381– 2385.

[41] K. S. Ramaiah, R.D. Pilkington, A.E. Hill, R.D. Tomlinson, A.K. Bhatnagar, "*Structural and optical investigations on CdS thin films grown by chemical bath technique*", **Mater. Chem. Phys.**, **68**, (2001), 22–30.

[42] T. Pisarkiewicz, E. Schabowska-Osiowska, and E. Kusior, "*Cadmium sulfide thin films manufactured by chemical bath deposition method*", **J. Wide Bandgap Mater**., **9**, (2001), 127-132.

[43] Isaiah, Oladeji, and LeeChow, "*Optimization of chemical bath deposited cadmium sulfide thin films*", **J. Electrochem. Soc.**, **144**, (1997), 2343-2346.

[44] J. Aguilar-Hernández, J. Sastre-Hernández, N. Ximello-Quiebras, R. Mendoza-Pérez, O. Vigil-Galán, G. Contreras-Puente, and M. Cárdenas-García, "*Influence of the S/Cd ratio on the luminescent properties of chemical bath deposited CdS films*", **Sol. Energy Mater. Sol. Cells**, **90,** (2006), 2305–2311.

[45] O. Vigil-Galán, A. Morales-Acevedo, F. Cruz-Gandarilla, and M.G. Jiménez-Escamilla, "*Characterization of CBD–CdS layers with different S/Cd ratios in the chemical bath and their relation with the efficiency of CdS/CdTe solar cells*", **Thin Solid Films**, **515,** (2007), 6085–6088.

[46] M. A. Martínez, C. Guillén, J. Herrero, "*Morphological and structural studies of CBD-CdS thin films by microscopy and diffraction techniques*", **Appl. Surf. Sci**., **136**, (1998),8.

[47] M. Rami, E. Benamar, M. Fahoume, F. Chraibi, A. Ennaoui, "*Effect of the cadmium ion source on the structural and optical properties of chemical bath deposited CdS thin films*", **Solid State Sci**., **1.1** ,(1999), 179.

[48] F.A. Cotton, G. Willkinson, "**Advanced Inorganic Chemistry**", 4th edn., Wiley, New York, 1980.

[49] H. S. Hilal, R. M.A. Ismail, A. El-Hamouz, A. Zyoud, I. Saadeddin, "*Effect of cooling rate of pre-annealed CdS thin film electrodes prepared by chemical bath deposition: Enhancement of photo-electrochemical characteristics*", **Electrochim. Acta**, **54,** (2009), 3433–3440.

[50] J.K. Dongre, V. Nogriya, M. Ramrakhiani, "*Structural, optical and photo-electrochemical characterization of CdS nanowire synthesized*

by chemical bath deposition and wet chemical etching", **Appl. Surf. Sci.**, **255**, (2009), 6115–6120.

[51] V. D. Das, J. Sathyanarayanan, and L. Damodare, *"Effect of annealing and surface treatment on the efficiency of photoelectrochemical (PEC) solar cells with vacuum-deposited n-InSe thin film electrode"*, **Surf. Coat. Technol.**, **94-95** , (1997), 669-671.

[52] H. El Malikia, J. C. Bernédea, S. Marsillaca, J. Pinelb, X. Castelb, and J. Pouzeta, *"Study of the influence of annealing on the properties of CBD-CdS thin films"*, **Appl. Surf. Sci.**, **205**, (2003), 65–79.

[53] R. Lozada-Morales, O. Zelaya-Angel, G. Torres-Delgado, *"Photoluminescence in cubic and hexagonal CdS films"*, **Appl. Surf. Sci.**, **175-176**, (2001), 562–566.

[54] K.V. Zinoviev, O. Zelaya-Angel, *"Influence of low temperature thermal annealing on the dark resistivity of chemical bath deposited CdS films"*, **Mater. Chem. Phys.**, **70,** (2001), 100–102.

[55] E. Çetinörgü, C. Gümüş, R. Esen, *"Effects of deposition time and temperature on the optical properties of air-annealed chemical bath deposited CdS films"*, **Thin Solid Films**, **515,** (2006), 1688–1693.

[56] Sh. Mishra, A. Ingale , U.N. Roy, A. Gupta, *"Study of annealing-induced changes in CdS thin films using X-ray diffraction and Raman spectroscopy"*, **Thin Solid Films**, **516,** (2007), 91–98.

[57] H. Metina, R. Esenb, "*Annealing studies on CBD grown CdS thin films*", **J. Cryst. Growth**, **258,** (2003), 141–148.

[58] A. S. N. Murthy and K. S. Reddy, "*Photo-electrochemical studies on polycrystalline CdS (chemical bath deposition) and CdSe (chemical bath and electrodeposition) thin film electrodes*", **J. Power Sources,** **13,** (1984), 159 – 167.

[59] F. Goto, K. Shirai, M. Ichimura, "*Defect reduction in electrochemically deposited CdS thin films by annealing in O_2*", **Sol. Energy Mater. Sol. Cells**, **50**, (1998), 147–153.

[60] C. Guillén, M. A. MartõÂnez, J. Herrero, "*Accurate control of thin film CdS growth process by adjusting the chemical bath deposition parameters*", **Thin Solid Films**, **335**, (1998), 37–42.

[61] K. S. Ramaiah, R. D. Pilkington, A. E. Hill, R.D. Tomlinson, A.K. Bhatnagar, "*Structural and optical investigations on CdS thin films grown by chemical bath technique*", **Mater.Chem. and Phys.**, **68**, (2001), 22–30.

[62] T. Zhang, X. Zhang, L.Ding, W. Zhang, "*Study on resistance switching properties of $Na_{0.5}Bi_{0.5}TiO_3$ thin films using impedance spectroscopy***, Nanoscale Research Letters, 4,** (2009).

[63] V. D. Das, J. Sathyanarayanan, and L. Damodare, "*Effect of annealing and surface treatment on the efficiency of photoelectrochemical (PEC) solar cells with vacuum-deposited n-*

InSe thin film electrode", **Surf. Coat. Technol.**, **94-95**, (1997) 669-671.

[64] R. Singh, M. Fakhruddin, K.F. Poole, "***Rapid photothermal processing as a semiconductor manufacturing technology for 21st century***", **Appl. Surf. Sci**., **168** (2000), 198–203.

[65] H. Fujioka, J. Ohta, H. Katada, T. Ikida, Y. Noguchi, M. Oshima, "***Epitaxial growth of semiconductor on SrTiO_3 substrates***", **J. Cryst. Growth**, **229** (2001), 137–141.

[66] A. Claverie, B. Colombeau, G. B. Assayage, C. Bonafos, F. Cristiano, M. Omri, B. Mauduit, "***Thermal evolution of extended defects in implanted Si: Impact on dopant diffusion***", **Mater. Sci. Semicond. Process**., **3**, (2000), 269–277.

[67] L. Whang, X. Huang, Z. Ma, Z. Li, J.Shi, L. Zhang, Y. Bao, X. Wang, W. Li, J. Xu, K. Chen, "***Thermal annealing of a-Si:H=a-SiNx:H multilayers***", **Appl. Phys. A.**, (2001).

[68] T. Kitanani, M. Kondow, T. Tanaka, "***Effect of thermal annealing procedure and a strained intermediate layer on a highly-strained GaInNAs=GaAs double-quantum-well structure***", **J. Cryst. Growth**, **221**, (2000), 491–495.

[69] T. Kitatani, K. Nakahara, M. Kondow, K. Uomi, and T. Tanaka, "***Mechanism analysis of improved GaInNAs otical properties through thermal annealing***", **J. Cryst. Growth**, **209,** (2000), 345-349.

[70] R. Singh, M. Fakhruddin, and K. F. Poole, "*Rapid photothermal processing as a semiconductor manufacturing technology for 21st Century*", **Appl. Surf. Sci.**, **168,** (2000), 198-203.

[71] H. Fujioka, J. Ohta, H. Katada, T. Ikida, Y. Noguchi, and M.Oshima, "*Epitaxial growth of semiconductor on SrTiO₃ substrates*", **J. Cryst. Growth**, **229**, (2001), 137-141.

[72] I. Sadeddin, " **Modification of semiconductor electrode characteristics by annealing and cooling at different rates**", Master's Thesis, An-Najah National University, Nablus, Palestine, (2002), p.63.

[73] S. H. Yoon, S. S. Lee, K. W. Seo, and Il-W. Shim, "*Preparation of CdS thin films through MOCVD method, using Cd-S single-source precursors*", **Bull. Korean Chem. Soc**., **27,** (2006), 2072.

[74] N.-H. Kim, S.-H. Ryu, H.-S. Noh, W.-S. Lee, "*Electrical and optical properties of sputter-deposited cadmium sulfide thin films optimized by annealing temperature*", **Mater. Sci. Semicond. Process**., In Press (2011).

[75] M. Majumder, A. K. Chakraborty, B. Mallik, "*Photoluminescence studies on nanostructured cadmium sulfide thin films prepared by chemical bath deposition method and annealed at different temperatures*", **J. Lumin**., **130**, (2010), 1497–1503.

[76] See Ref. [16], p. 32-38.

[77] See Ref.[20], p.82.

[78] V. S. Taur, R. A. Joshi, A. V. Ghule, R. Sharma, "*Effect of annealing on photovoltaic characteristics of nanostructured p-Cu2S/n-CdS thin film*", **Renew. Energ**., **38**, (2012), 219-223.

[79] See Ref. [20], p.85.

جامعة النجاح الوطنية

كلية الدراسات العليا

أفلام CdS الرقيقة كأقطاب فوتوكهروكيميائية: التحضير بالجمع بين الترسيب الكيميائي والكهروكيميائي

إعداد

سحر مصطفى أسعد خدرج

إشراف

أ.د. حكمت هلال

د. إياد سعد الدين

قدمت هذه الرسالة استكمالاً لمتطلبات الحصول على درجة الماجستير في الكيمياء بكلية الدراسات العليا في جامعة النجاح الوطنية في نابلس، فلسطين.

2011م

أفلام CdS الرقيقة كأقطاب فوتوكهروكيميائية:

التحضير بالجمع بين الترسيب الكيميائي والكهروكيميائي

إعداد

سحر مصطفى أسعد خدرج

إشراف

أ.د. حكمت هلال

د. إياد سعد الدين

الملخص

تم تحضير أفــلام CdS الرقيقــة النانويــة علــى شــرائح مــن الزجـاج الموصـل (FTO/coated) باستخدام طرق مختلفة منهـا الترسـيب الكهروكيميـائي (EC) والترسـيب الكيميائي (CBD) ثم طريقة الجمع بين الطريقتين سابقتي الذكر، حيث يتم اسـتخدام الطريقـة الأخيرة للمرة الأولى في عملية التحضير.

كما تم دراسة خصائص الأفلام المحضرة باستخدام طرق مختلفة منها أطياف انحـراف أشــعة إكــس (X-Ray diffraction) وأطيــاف الامتصــاص (electronic absorption spectra) وأطياف الوميض (PL spectra) والمجهر الالكتروني الماسح (SEM).

أظهرت نتائج التصوير بواسطة المجهر الالكتروني الماسح صــورا مختلفــة للأفــلام المحضرة. بينما أثبتت اطياف الامتصاص انه لا يوجد اختلاف كبير بين الافلام المحضرة. أمــا أطياف الوميض فقد أظهرت أنماطا متماثلة للأفلام المحضرة بالطرق المختلفة.

لقد تم دراسة خصائص كافة الأفلام المحضرة في تحويل الضوء الى كهرباء بالطريقــة الفوتوكهروكيميائية، وقد بنيت هذه الدراسة على أساس قياس عدة عوامل مثل منحنيــات كثافــة تيار الظلمة (dark current density) مقابل الجهد، منحنيات كثافة تيــار الإضــاءة (photo current density) مقابل الجهد، كثافة تيارات الــدارة القصــيرة (short circuit current density)، جهد الدارة المفتوح (open circuit voltage)، كفاءة الخلية في تحويل الضوء إلى كهرباء (conversion efficiency). وتمت هذه الدراسات بالتوازي مع دراسة نتائج التصوير

بواسطة الماسح الميكروسكوبي الإلكتروني (scanning electron microscopy) ومطيـــاف اشعة اكس للأفلام المحضرة.

هذا وقد أظهرت الدراسة الفوتوكهروكيميائية للأفلام المحضرة بالطرق المختلفة ســـلوكا ومسارات مختلفة، حيث وجد أن الخلية الفوتوكهروكيميائية للأفلام المحضرة بطريقــة الجمـــع أعلى كفاءة من خلية الأفلام المحضرة بطريقة الترسيب الكهروكيميائي، وأقل من خلية الأفـــلام المحضرة بطريقة الترسيب الكيميائي. وقد حققت الافلام المحضرة بطريقة الجمع أكثر ثباتية في مقاومة التحطم الضوئي مع الزمن مقارنة بنظيرتيها المحضرتين بطريقة الترسـيب الكيميـــائي والترسيب الكهروكيميائي.

علاوة على ما سبق، تم دراسة تأثير الشيِّ (التسخين) عند درجة حـــرارة 250 مئويـــة وعملية التبريد البطئ على خصائص الأفلام المحضرة، وقد وجد أن الأفلام المشـــوية أفضـــل كفاءة في تحويل الضوء إلى كهرباء مقارنة بنظائرها غير المشوية. في حـــين أظهـــرت نتـــائج التصوير بواسطة المجهر الالكتروني الماسح أن عملية الشي قد زادت حجم حبيبـــات كبريتيـــد الكادميوم (nano-particles) للأفلام المحضرة. أما نتائج انحراف أشعة إكس فقد أظهـــرت أن عملية الشي تقلل من حجم البلورية للافلام الكهروكيميائية وتزيد من حجـــم البلوريـــة للافـــلام المرسبة كيميائيا و الافلام المحضرة بطريقة الجمع. أما نتـــائج أطيـــاف الامتصـــاص وقيـــاس الوميض فقد أظهرت عدم تأثر طول موجة الامتصاص أوالانبعاث الافلام بعملية الشـــي علـــى الترتيب.

على صعيد آخر، وجد أن الشي قد حسن منحنيات تيار الإضاءة مقابل الجهـــد لأفـــلام كبريتيد الكادميوم الرقيقة المحضرة بطريقة الجمع في الأنظمة الفوتوكهروكيميائية بطريقة أفضل مقارنة بنظيرتيها المحضرتين بطريقة الترسيب الكيميائي والكهروكيميائي حيث وجد أن الخليـــة الفوتوكهروكيميائية للأفلام المشوية المحضرة بطريقة الجمع أفضل كفاءة في تحويل الضوء إلى كهرباء مقارنة بنظيرتيها المحضرتين بطريقة الترسيب الكيميائي والكهروكيميائي وأكثر ثباتيـــة في مقاومة التحطم الضوئي مع الزمن.